

Fleur Kettner

Numerical modelling of flow over spillways

D1-2010-12

Trondheim, June 2010

UTTAK AV MASTEROPPGAVE

Navn: Fleur Kettner	Student nr.
Study program: <i>Civil and Environmental Engineering</i> x <i>Ingeniørvitenskap og IKT</i> <input type="checkbox"/> <i>Produktutvikling og produksjon</i> <input type="checkbox"/>	
Area of study: River Engineering	
Title (Norwegian): Numerisk modellering av strømning over overløp Title (English): Numerical modelling of flow over spillways	
Teacher: Nils Reidar B. Olsen	
Supervisor: Nils Reidar B. Olsen	
Date given: 18/1 2010	
Submission date: 14/6 2010	
Special information (gruppeoppgave, oppgave utenom NTNU etc.): The student will make the thesis at NTNU as a part of a study programme at the University of Karlsruhe	
Signature teacher: ----- dato	----- signature
Signature student: (I confirm having read the regulations applying to the MSc thesis) ----- dato	----- signature
Verified by the department administration: ----- signature	

Numerical modelling of flow over spillways

Background

Computing the capacity of spillway is an important part of the design in hydropower dam engineering. Until recently, such investigations were done by use of physical model studies. The last few years have seen the emergence of the use of computational fluid dynamics to compute the spillway capacity. The research for the current thesis will look at this problem.

A physical model of the dam Sarpfossen is currently being built at NTNU. Measurements of the water level and discharges from this model are to be used in the current study. It might also be possible to measure water velocities in the model using ADV's. The measurements are to be used in testing a commercial CFD program, to see how well it can replicate the flow conditions and discharge capacity predictions from the physical model. The commercial CFD program will be either FLOW-3D or STAR-CCM+. These programs use a volume of fluid (VOF) method on a fixed grid to compute the location of the free water surface. In addition to using the commercial programs, the NTNU developed program SSIIM will be used. The SSIIM program uses a newly developed algorithm to predict the free water surface using the continuity equation together with the pressure from the SIMPLE method. An adaptive grid is used instead of the VOF/fixed grid method, requiring less cells or lower computational time. The new algorithm will be tested on simplified lab cases and it can also be tested on the Sarpfossen model, if time permits.

Important questions in the thesis

The thesis will answer the following questions:

- How can a grid be made for the spillway of Sarpfossen dam?
- How are input-data made for a computation with the commercial CFD program for Sarpfossen dam?
- What will the computed velocity field be at the spillway of Sarpfossen dam?
- What will the computed water surface profile be for the spillway of Sarpfossen dam?
- How well do the results from the commercial CFD program fit with the measurements from the laboratory?
- What is the effect of uncertainties in the input data on the computational results?
- What is the effect of different algorithms in the commercial CFD program on the final result?

The conclusion of the thesis should include the opinion of the student about the usability of the CFD programs in computing the discharge capacity of spillways. It should also point to possible uncertainties in the numerical models and typical input data. The thesis should include recommendations for using numerical models on spillway capacity computations.

Supervision and reporting

The main supervisor for the thesis will be Prof. Nils R. Olsen, who will also give advice on the SSIIM program. Dr. Robert Feurich will give advice on the commercial CFD program. The student will work in the CFD group of the river engineering group at the NTNU, and can also get advice from other researchers, for example Dr. Nils R  ther or Hans Bihs.

A professional structuring of the thesis is important. The thesis should include a table of content, a table of figures and a list of references. The thesis should contain dominantly black and white line drawing as figurer, for example of grids, velocity vectors and comparisons between computed and measured values. Colour figures can be used for important parameters.

In addition to paper copies of the thesis, a CD must be handed in with a PDF file and a Word/Framemaker file of the thesis. The CD must also include the figures from the thesis and the most important input files for the CFD computations.

Assume that the reader of the thesis is a river engineer with some knowledge of numerical modelling, but without detailed knowledge of the specific computer programs used in the study.

This text has to be included in the thesis. It will be used in the grading of the thesis.

Acknowledgements

I want to express my gratitude to several people who supported me in accomplishing my thesis. Prof. Nils Reidar Olsen gave guidance in all aspects of the thesis. His patience and most important advices supported me extremely. Special thanks is also acknowledged to Prof. Markus Uhlmann who enabled me to write this thesis at the NTNU in Trondheim. I would also like to thank Dr. Robert Feurich for invaluable advices and encouragement throughout this thesis. Special thanks also to the staff of the Vassdragslaboratoriet at NTNU, especially Geir Tesaker and Torgeir Jensen who always gave me a helping hand in the laboratory. Despite of being abroad, my parents always encourage me and I like to thank them for their support in all respects. I also like to thank Olav for his lovely encouragements.

Abstract

The spillway of Sarpfossen hydropower plant has been studied numerically and experimentally. The physical model was built in the Vassdragslaboratoriet at the Norwegian University of Science and Technology, NTNU. The model consists of the Sarpfossen dam and the river Glomma upstream of the dam. On the spillway crest are three gates installed - two flap gates and a sector gate. In addition is further upstream of the dam a bridge for cars and trains. Two of the bridge piers are fixed in the water and has an influence in the flow pattern. The model was run with a certain discharge and the velocities in the river were measured with a Flow Meter and Vectrino Velocimeter. Besides of the velocity measurements the water levels between bridge and dam were measured. These measurements were conducted to investigate the occurring wave phenomena, shock wave. The simulations were carried out by a commercial program, STAR-CCM+. The results from the simulation have been verified by the measurements from the model.

Simulation were performed to replicate the flow phenomenas in the physical model and to find out how well STAR-CCM+ is suited to cope the complex flow structures. Three simulations were performed - two for the velocity distribution and one for the water level measurements with generated shock waves. The results of the simulations show quite good correlations. The velocity measurements show satisfying results. The shock wave could also be replicated quite well and the results are quite promising.

Future studies are recommended to get more experience with simulating complex free-surface flows. Especially simulations of shock wave are not very frequent and well tested and should be included in further studies.

LIST OF SYMBOLS

Symbol	Definition
g	Gravitational acceleration
i	Grid points
k	Kinetic energy
n	Time-step
s_α	Source or sink term
r	relaxation factor
x, y, z	Physical space coordinate
u	Velocity in x-direction
\mathbf{u}	Velocity vector, $\mathbf{u} = (u, v, w)$
$\langle u \rangle$	Mean velocity
u'	Velocity fluctuation
u_{VV}	Velocity Vectrino Velocimeter in x-direction
v	Velocity in y-direction
v_{VV}	Velocity Vectrino Velocimeter in y-direction
w	Velocity in w-direction
w_{VV}	Velocity Vectrino Velocimeter in z-direction
p	Pressure
α	Volume fraction
δ_{ij}	Kronecker delta, $\delta_{ij} = \begin{cases} 1 & \text{if } i = j \\ 0 & \text{if } i \neq j \end{cases}$
∇	Nabla-Operator, $\nabla = \left(\frac{\partial}{\partial x}, \frac{\partial}{\partial y}, \frac{\partial}{\partial z} \right)$
ν	Kinematic viscosity
ν_t	Turbulent viscosity
μ	dynamic viscosity
ρ	density of water
σ_ϵ	K - ϵ constant = 1.3
ϵ	Dissipation term
σ_ϵ	Turbulent Prandtl number = 1
C_{ϵ_1}	K- ϵ constant = 1.44
C_{ϵ_2}	K- ϵ constant = 1.92
C_μ	0.09
a_{ij}	Anisotropy tensor
S_{ij}	Rate-of-strain tensor
a.s.l.	above sea level
CFD	Computational Fluid Dynamic
DNS	Direct numerical simulation
LES	Large Eddy Simulation
RANS	Reynolds-Averaged Navier-Stokes equation
Re	Reynolds number
STL	Stereolithography
TKE	Turbulent kinetic energy
Tdr	Turbulent dissipation rate
VOF	Volume Of Fluid

Contents

Acknowledgements	i
Abstract	iii
LIST OF SYMBOLS	vi
LIST OF FIGURES	x
LIST OF TABLES	xi
1. INTRODUCTION	1
1.1. Motivation	1
1.2. Terms of References	2
2. PHYSICAL MODEL	3
2.1. Construction	3
2.2. Dam	3
2.2.1. Spillway	4
2.2.2. Sector Gate	5
2.2.3. Flap Gate	6
2.3. Task	7
3. MEASUREMENTS OF THE WATER VELOCITY	9
3.1. Flow Meter	10
3.2. Vectrino Velocimeter	11
3.3. Evaluation of the measurements	14
3.4. Errors accompanying the measurements	17
4. SHOCK WAVES	19
4.1. Definition	19
4.2. Measurements Of Shock Waves	20
5. NUMERICAL MODEL	23
5.1. Introduction to Turbulence	23
5.2. Computational Fluid Dynamic	23
5.3. Navier-Stokes Equation	24
5.4. RANS	25
5.5. Turbulence Model	25
5.6. Discretization Scheme	27
5.7. VOF	28
5.8. Characteristics of Numerical Methods	28
5.9. Source of Errors and Uncertainties	29
6. SOFTWARE	31
6.1. AutoCAD	31

6.2. STAR-CCM+	32
6.2.1. General features	33
6.2.2. Pre-Processing	33
6.2.3. Solving	38
6.2.4. Post-Processing	39
6.3. Mesh Generation	40
6.3.1. The Choice of Mesh	40
7. RESULTS	43
7.1. Velocity Distribution	43
7.1.1. Polyhedral Mesh	44
7.1.2. Trimmed Mesh	47
7.1.3. Discussion	49
7.2. Shock waves	50
7.2.1. Discussion	51
8. CONCLUSION	55
9. RECOMMENDATIONS	57
9.1. Vectrino Velocimeter	57
9.2. STAR-CCM+	57
REFERENCES	59
A. Data sheet	61
B. Example: Simulation properties (for shock waves)	64

List of Figures

2.1. View of the physical model in the Vassdragslaboratoriet at NTNU	3
2.2. Downstream view of the stilling basin in Sarpsborg, photo: G.Tesaker	5
2.3. Sector gate	6
2.4. Flap gate	7
3.1. Flowchart showing the processes occurring in a measurement system, [1]	9
3.2. Flow Meter Model 801	10
3.3. Cross-section close to inflow with the selected measuring points	11
3.4. Vectrino Velocimeter with a side-looking probe	12
3.5. Positioning the Vectrino Velocimeter above a measuring point, photo: N. Olsen	13
3.6. Graphical view of the velocities at point 8 in cross-section 23	13
3.7. Probe check of point 10 in cross-section 23	14
3.8. Overview of the cross-sections and measuring points for the Vectrino measurements	15
3.9. Vectrino Velocimeter positioned above a measuring point along the cross-section showing the coordinate system	16
3.10. Decomposition of the velocity along a cross-section	16
4.1. Shock Waves in channel contraction, [2]	20
4.2. Cross-sections and measuring points for the shock waves	21
4.3. Overview of observed and measured shock waves	22
6.1. Example: Creating the geometry for STAR-CCM+ on one part of the cross-sections	32
6.2. Scalar scene: Overflow over dam by applying the Volume Fraction of H2O ((a)-(b)), Reservoir ((c))	35
6.3. Different mesh types	36
6.4. Derivation of the normal direction of the plane sections	40
6.5. Overview of a structured and unstructured mesh	41
6.6. Difference between orthogonal (left) and non-orthogonal mesh (right), [3]	41
7.1. Velocity distribution for the trimmed mesh, downstream view (a)-(c), upstream view (d)	44
7.2. Measured and calculated velocities with water surface and river bed of cross-section 23	44
7.3. Measured and calculated velocities with water surface and river bed of cross-section 36	45
7.4. Measured and calculated velocities with water surface and river bed of cross-section 51	46
7.5. Measured and calculated velocities with water surface and river bed of cross-section 36	47

7.6. Measured and calculated velocities with water surface and river bed of cross-section 36	48
7.7. Measured and calculated velocities with water surface and river bed of cross-section 51	48
7.8. Residual plots	49
7.9. Shock wave	50
7.10. Water level graphs of the measured (blue) and calculated values(rosa)	52
7.11. Residual plot of the shock wave simulation	53
 A.1. Data sheet	 61
A.2. Data sheet	62
A.3. Data sheet	63

List of Tables

3.1. Settings of the Vectrino Velocimeter	12
6.1. Boundary types used in the simulation	33
6.2. Physics Conditions of each boundary type	34
6.3. Values for the Field Function for closed and open gate position	35
6.4. Selected Meshing Models	36
6.5. Physics Models. Overview of the selected model and alternative models	38
6.6. Solver parameters	39

1. INTRODUCTION

The ability of controlling water for the production of energy has a long history. Especially in Norway where hydropower corresponds to the most important source of energy. Around 98 % of the energy supply Norway is able to cover with hydropower. One of the 850 existing hydropower stations is located in Sarpsborg which was put into operation in 1899. It is owned by Hafslund Produksjon AS and Borregård AS. The Sarpfossen dam regulates the river Glomma, Norway's longest and widest river. The river water passes on its long way (601 km) from the source close to Røros to Fredrikstad, where the water enters the Oslofjord, the city Sarpsborg. Glomma covers an altitude difference of 860 a.s.l and has an average flow rate of $425 \text{ m}^3/\text{s}$. The dam is made out of concrete and on the crest are three gates located - two flap gates and a sector gate on the east side. The spillway has a height of 20.5 m. Upstream of the dam is a car- and train bridge. This bridge pier also have an influence in the flow condition.

The owner of the power plant commissioned the physical model to get information for the design of a new power station. The physical model consists of the dam construction, the bridge upstream of the dam and the reservoir as well as a stilling basin downstream of the dam construction. The model reservoir has an area of approximately 166 m^2 . Experiments will be carried out over the next months to improve the flow situation in case of a flood. These measurements are conducted by the staff of the Vassdragslaboratoriet and are not part of this thesis. All the dimensions of the structures like gates, dam and bridge piers were measured in the Vassdragslaboratoriet. The data of the cross-sections were provided by Svein Vold and were measured in the prototype. For the thesis the physical model was used to do the measurements with which the commercial program, STAR-CCM+, was tested.

1.1. Motivation

Conducting measurements in the physical model is commonly used and are an essential part in the field of research. One task of the thesis was to measure the water velocity in the reservoir. Over the last year more precise measuring instruments for the water velocity have been developed and a wide range of different measuring systems exists. For this thesis a Vectrino Velocimeter was used which was provided by the Vassdragslaboratoriet. The Vectrino Velocimeter enables three-dimensional velocity measurements. Because of the special river geometry, a contraction starting from the bridge occur. This contraction causes shock waves which are an important, but not well investigated flow phenomena. To catch these special wave features measurements were conducted manually.

In the last years, numerical simulation programs were used to investigate how well the flow phenomena can be replicated. Developing a CFD software which is able to calculate variables, like pressure or velocities, accurately and with a high reliability is nowadays not possible. Testing CFD program by comparing measurements from the physical model help to avoid further errors and uncertainties.

The main purpose of this thesis is to test the CFD program STAR-CCM+ with the data measured in the physical model. STAR-CCM+ was chosen, because it consists of features which consider a free water surface. Additionally, STAR-CCM+ is based on an orthogonal and non-orthogonal mesh. This thesis includes the discussion of the results obtain by comparing the measurements with the calculated values. Moreover recommendations are given which could be useful for further studies.

1.2. Terms of References

The thesis consists of the following 6 chapters:

Chapter 1 gives information about the prototype and the dam construction. Moreover a short description of the thesis task is given.

Chapter 2 describes the physical model with the focus on the component parts. The term dam and spillway is explained further as well as the different gates types. Finally the task of the thesis is explained more accurately.

Chapter 3 introduces the different measuring instruments used to determine the water velocity. The manipulation of the measurement values are described. Potential error sources which might have accomplished the measurements are given at the end of the chapter.

Chapter 4 deals with the wave phenomena shock wave. The characteristic of the shock waves is mentioned followed by the description of the manipulation of the measurements.

Chapter 5 gives an insight in the world of numerics. The terms Turbulence, Navier-Stokes equation, Reynolds-Averaged Navier-Stokes equation and Turbulence model are explained. Furthermore the discretization schemes and the theory of VOF are described. Finally, some Characteristics of Numerical Methods with their errors and uncertainties are mentioned.

Chapter 6 gives an deeper look on the softwares used for accomplishing this thesis. The focus is on AutoCAD and STAR-CCM+. The reason why AutoCAD was used and the steps to generate the geometry for STAR-CCM+ is mentioned. STAR-CCM+ is described by the tools used for setting up the simulations. STAR-CCM+ is described by the Pre-Processing paragraph, containing boundary and mesh types, Physics Conditions, Field Function and Physics Models. The Pre-Processing is followed by the Solvers which contains the Time-Step, the different parameters of the Discretization Scheme and Relaxation Factors. Additionally the Post-Processing tool are described explaining Iso-Surface and Plane Sections and how to export data from the simulation. Finally different Mesh Structures are mentioned including the description of the terms Body-fitted and Nested Mesh.

Chapter 7 describes the Results obtained by comparing the measurements with the calculations. The simulations of the Velocity Distribution were conducted on an Orthogonal and Trimmed Mesh. The Results are compared and deviations are explained. A Discussion of the two mesh types follows at the end. The Results from the Shock Wave are shown and discussed.

Chapter 8 is the Conclusion chapter and deals summarize the measurements in the physical model and the simulations.

Chapter 9 includes some recommendations to improve the Results in further work.

The list of References and the input data and parameters to set up the simulations complete this thesis.

2. PHYSICAL MODEL

2.1. Construction

The physical model was finished in April, 2010. The staff of the Vassdragslaboratoriet built the model on a scale of 1:45. The natural river bed consists of rocks and to ensure a similar roughness in the physical model the bed is made of concrete. The Vassdragslaboratoriet which was established in the year 1958 is equipped with three pump systems. Each pump system consists of two pumps - a 200 l/s and 100 l/s pump. The change of the gate openings is very simple and can be done manually by lifting the gates up or down. Figure 2.1 shows the physical model as viewed from the downstream side.

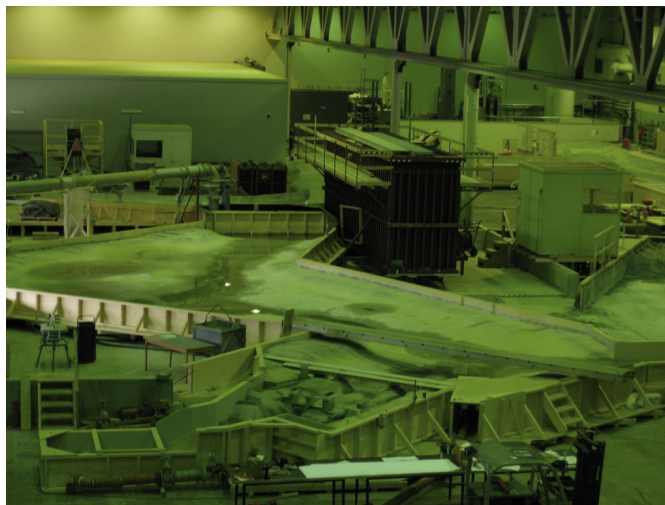


Figure 2.1.: View of the physical model in the Vassdragslaboratoriet at NTNU

2.2. Dam

Dam constructions are unique due to different standards at each location, but also in respect of the impacts, e.g. on geophysical aspects like slope stability or sediment transport, which accompany the constructions and also has to be focused on. For the design of dam constructions a wide range of engineering fields have to be integrated to cover the geotechnical, geological, material, hydrological and hydraulic regulations [4].

The main purpose of dams is to store and control the water safely. There are two categories of dam - embankment or concrete dams. Because the Sarpfossen dam is built of concrete only this type is described further. Concrete dams are only a hypernym of the following types: Buttress,

Arch and Gravity dams. The stability of the Sarpfossen dam is ensured by the dam geometric shape and mass which are typical factors for gravity dams. The demands on the materials for producing concrete which fulfill an adequate quality are high and are for stability reasons very important. Moreover, an appropriate shear strength in the bed is necessary to avoid any dam movements. Three stability criteria exist [5]:

- **Overturning**
Overturning is characterized by rotational processes. The stability is defined as the ratio of stabilizing moments (including weight loads) to destabilizing moments (water load). The ratio should be greater than 1.5. For intact dam is overturning not a serious problem.
- **Sliding**
Sliding is also known as translation. The sliding criteria expresses the ratio of the summarized horizontal loads to the summation of the vertical acting loads. It can be specified due to cohesion and frictional resistance to shearing ($\tan \varphi$), where φ expresses the internal friction. A table for these values exists according to the different dam types
- **Material failure** Material failure can occur if the concrete of the dam has a bad quality.

A part of the dam construction is the spillway design which will be introduced in paragraph 2.2.1.

2.2.1. Spillway

The main principles of spillways is to protect the dam and gates by leading the design flood safely downstream and overtopping has to be avoided. This situation, when flood water has to pass the dam construction is a very critical aspect and it affords a high understanding in dam construction [5]. A relevant parameter for spillways is the spillway capacity which must correspond to the maximum design discharge. The capacity of spillways is therefore relevant for the regular operation, but also for the safety in case of floods [5]. The Sarpfossen dam is located in a narrow part of the river flow and the passing or overflowing water is falling in a stilling basin. The stilling basin is naturally formed with a very rocky structure to ensure the dissipation of the kinetic energy. The rocks however, are reinforced by concrete. When the water is passing the dam crest down over the spillway the water velocity increases rapidly and supercritical flow is achieved. The main task of the stilling basin is to convert the flow characterized by a high kinetic energy into a subcritical flow by an oblique hydraulic jump, also known as shock waves, which is associated with significant energy losses. In addition to the energy dissipation the stilling basin also ensures the stabilization of the shock waves at one position. The stilling basin of the

prototype is shown in Figure 2.2.



Figure 2.2.: Downstream view of the stilling basin in Sarpsborg, photo: G.Tesaker

The spillway is classified as controlled and consists in contrast to the uncontrolled spillway of gate constructions. In the following the two types of overflowing gates which are installed in the Sarpfossen dam will be introduced.

2.2.2. Sector Gate

The invention of gates and hence the possibility of varying the opening of dams make the operation of hydraulic structures more flexible and safe. Gates exist in a lot of different variants which can be classified according to the type of motion, moving mechanisms and the position in the dam [5]. The gates in the Sarpfossen dam belong to the crest gates and the design of is dependent on the pressure transfer. The pressure is transferred to the piers and sill. One of the crest gates is the sector gate and can be classified as a rotation gate which means that the gate rotates due to a hinge axis fixed on the downstream side. The sector gate is mounted on the east side of the dam.

The main components of sector gates are the vaulted upstream and downstream skin plates, which are mostly metal plates. The upstream skin plate mostly sticks out of the construction to increase the pressure level. The skin plates have to be designed for resisting high stresses and pressure variations. Therefore they are supported by vertical ribs and horizontal beams [6]. For adjusting the gate position a hydraulic motor is used generally. When the gate is in the lifted position, the water pressure keeps the gate up. The reservoir water can flow into a chamber, called buoyancy chamber, which is located in the crest below the gate and will raise the gate upwards by the resulting pressure. For lowering the gate the water in the buoyancy chamber has to stream out and the amount of outflowing water can be controlled by valves [7].

The sector gate in the Sarpfossen dam has a width of 27.9 m, height of about 7.5 m and radius of 10.8 m. The advantages of sector gates are that they can be easily controlled (mostly out of a control house), fast to move and are accurate in aspect of regulation. Furthermore, the gates ensure the safely passing of ice and debris by lowering the gate [5]. The gate can be completely moved down in the ground and the water with or without its load is able to pass the opening almost unhindered.

Fig. 2.3 shows the sector gate in the prototype compared to the measurements.

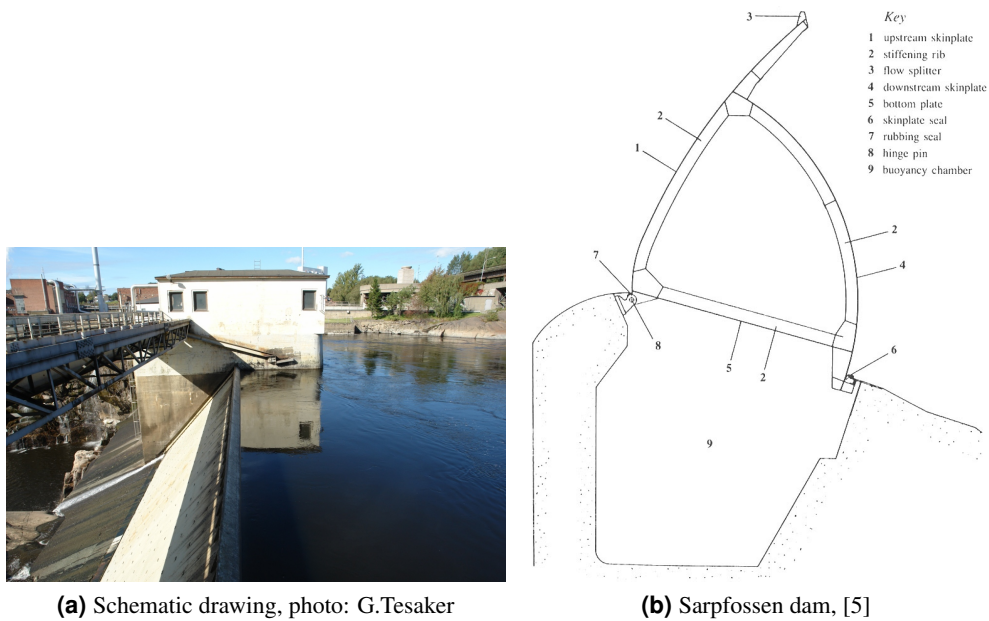


Figure 2.3.: Sector gate

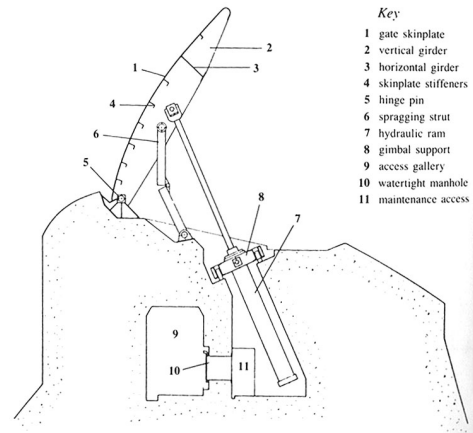
2.2.3. Flap Gate

Flap gates, also called bottom-hinged gates, counts also to the crest gates and is one of the simplest gate versions. This kind of crest gate is mostly used, not only because of the precisely regulation mechanism, but rather because of the ease of passing ice and debris safely over the dam. The advance regulation let the reservoir water flow downstream with a low water head. In aspect of the environment are the flap gates the most acceptable. Compared to the Sector gate the flap gate consists also of a skin plate, but only on the upstream side. The opening or closing process proceeds automatically. A small variation of the pressure on the back side is sufficient to lower the flap gate and water can flow over the dam. In contrary, when water on the front side is getting higher than on the back side the gate will close [7].

The flap gates are located on the right side in flow direction and both are about 5 m in height. Furthermore, each flap gate has a span length of around 13.5 m. The material of flap gates is mostly iron. In Fig. 2.4 the flap gate is shown as viewed from the downstream side.



(a) Downstream view of the Sarpfossen dam, photo: G.Tesaker



(b) Schematic drawing, [5]

Figure 2.4.: Flap gate

2.3. Task

The measurements were carried out relating to two different purposes. For the examination of the shock waves a high discharge was necessary to get a high Froude number and clearly formed shock waves to make the measurements even more simple. A discharge of 250 l/s was chosen with open gates. To ensure that the overflowing water had no impact on the shock waves measurements an outlet on the downstream side of the spillway was open. The discharge of the flow passing this outlet was 8 l/s. The total discharge was hence 242 l/s. How the shock waves were measured and to find out more about manipulation of the measurements values can be read in paragraph 4.2. For the velocity measurements in the reservoir a lower discharge of 100 l/s was set up and the measurements were conducted with maximum gate openings. Also for this case the outlet was open and the total discharge was 92 l/s. Close to the inflow the maximum velocity was needed for the boundary condition of the simulation. These measurements were collected with a Flow Meter, which is relatively simple to handle. Further velocity measurements were conducted on three more cross-section in the reservoir. Because the velocity should be measured three-dimensionally the Vectrino Velocimeter was used. More about the Flow Meter and the Vectrino Velocimeter as well as the evaluation of the measurement data can be read in chapter 3.

3. MEASUREMENTS OF THE WATER VELOCITY

In the last 100 years, the way of precise flow phenomena was getting more and more important and great improvements were achieved. There exists a huge variety of flow measuring instruments like Pitot tube, Prandtl tube, mechanical impeller, hot-wire anemometer and different Laser-based systems. The Pitot and Prandtl tube are simple measuring instruments which are based on the combination of static and dynamic pressure. Despite of its simplicity the Pitot tube is part in the sophisticated world of airplanes.

Also in the field of electrical engineering were measuring instruments, like the hot-wire anemometer, developed. Electrical instruments which combine electrical waves with magnetic waves are called electromagnetic instruments and are based on the Faraday principle. Electromagnetic waves are ubiquitous and include such phenomena as the visible light and radio waves. The measuring instrument, Flow Meter, which was one of the two used velocity measurement systems, is based on the electromagnetic principle and will be explained in the following paragraph.

Besides of the mentioned measurement principles represent the Acoustic Doppler Velocimeter another category of measurement systems. As indicated by its name, it uses the Doppler effect, which determines the water velocity based on a frequency shift resulting when a transmitted pulse is reflected by a suspended particle. The Vectrino Velocimeter, produced by Nortek AS, belongs to the Acoustic Doppler Velocimeter and was used for determining the water velocity in the reservoir of the physical model. Figure 3.1 shows the process which leads to the measuring value by using the Vectrino Velocimeter.

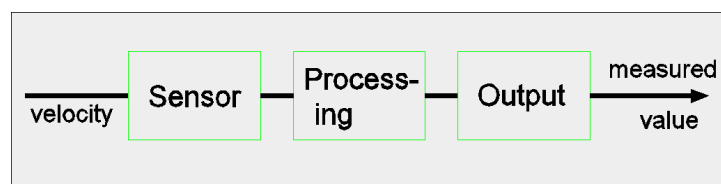


Figure 3.1.: Flowchart showing the processes occurring in a measurement system, [1]

The sensor is sensitive for the measuring parameter. For the Flow Meter the sensor is presented by the electrodes. The sensor of the Vectrino Velocimeter is defined by the probe head including the transmitter and the four receivers.

The following paragraphs include a closer look at the measurement systems used to obtain the water velocity.

3.1. Flow Meter

The Flow Meter is a single axis electromagnetic measurement instrument produced by Valeport. The Model 801 was used with a flat sensor which is in contact with the flow. The sensor generates an electromagnetic field which is passed by the water flow and has a certain energy. Hence, the flowing water induces a current which is measured by the electrodes. This principle was discovered by Faraday and is known as the Faraday's law [8]. Besides the sensor, the Flow Meter consists of a Control Display Unit, where the water velocity can be displayed in real time or averaged values. The velocity measurements are conducted within a cylindrical volume (20 mm \varnothing) which is positioned around the two electrodes and includes the area 10 mm above the sensor. The volume is relatively small and is hence adequate for measuring turbulent flows, which is indicated by noisy real time measuring values [8]. Figure 3.2 shows the Flow Meter with a flat sensor.

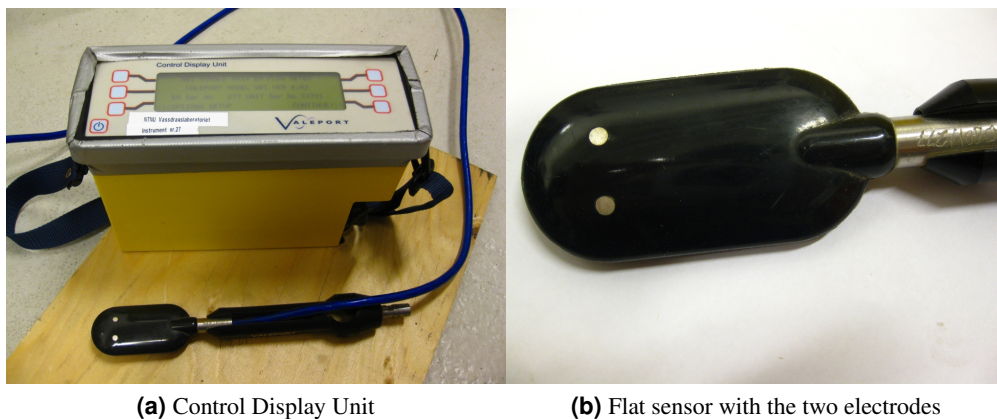


Figure 3.2.: Flow Meter Model 801

The Flow Meter was used to measure the maximum velocity near the inflow of the physical model.

The measuring instrument was mounted on a pole with the electrodes on top of the sensor which is measuring the flow above the sensor. The measurement instrument is relatively simple to use. The only difficulty was associated with finding the maximum velocity and several positions over the water depth of the Flow Meter had to be inspected. The points were marked on cross-section 3 as shown in Fig. 3.3: Cross-section 3 is sloped at an angle of $\varphi = -21^\circ$. For finding the coordinates of each point the provided coordinates of the cross-sections were imported in AutoCAD that will be further explained in paragraph 3.2. It has to be mentioned that the flow close to the inflow is very turbulent. The measurements conducted close to the inflow area could be used to model the inflow velocity distribution. The inflow cross-section is based on an uniform velocity distribution for the simulations of this thesis. The measurements should be used to define the boundary condition, but a simplified boundary condition was preferred to accomplish the thesis in time.

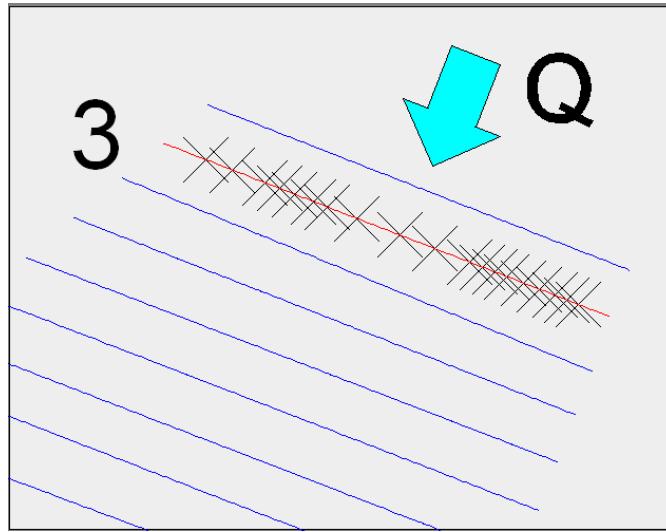


Figure 3.3.: Cross-section close to inflow with the selected measuring points

3.2. Vectrino Velocimeter

For the velocity measurements in the reservoir the Vectrino Velocimeter with a side-looking probe was used. The advantage of using this kind of measurement system is that the velocity is measured three-dimensionally and with a high resolution.

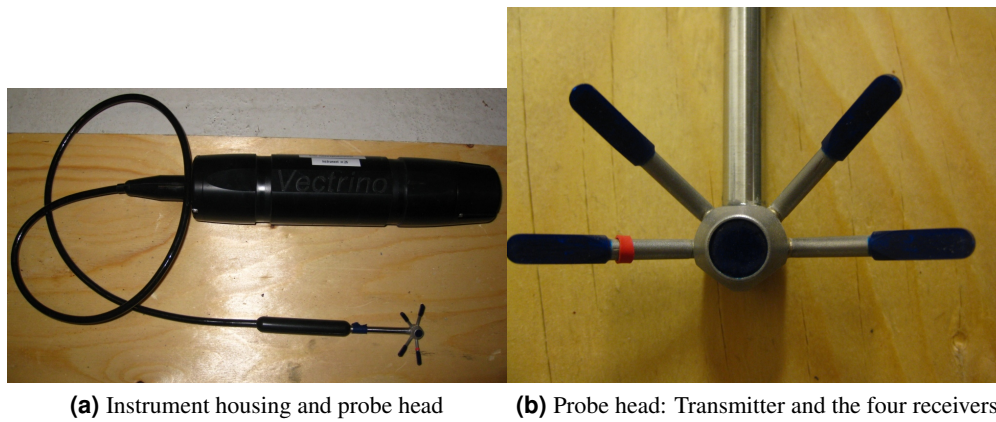
The Vectrino operates by sending out a pulse from the transmitter. The pulse is an ultrasonic wave which occurs in the range of more than 20,000 Hertz. The nature of ultrasonic waves is that the waves can be reflected at particles or interfaces. The transmitted pulse of the Vectrino Velocimeter is reflected within a sampling volume which includes suspended particles and is picked up by four receivers. The returned pulse has a shifted frequency compared to the transmitted pulse which describes a bistatic Doppler. Hence, the receiver arms are observing the superposition of both frequencies which is called Doppler shift [9]. The following equation shows the frequencies received by one of the receivers [10]:

$$F_m = F_0 - k_1 \mathbf{u} + k_2 \mathbf{u} \quad (3.1)$$

F_0 is the frequency of the transmitter, \mathbf{u} is the velocity perpendicular to the pulse, k_1 and k_2 are the wave number vectors.

The Doppler shift is proportional to the velocity of the suspended particles (or more exactly to the ratio of the velocity of the suspended particles to the velocity of the wave propagation). The suspended particles are small and are moving with the same velocity as the water. Hence the Vectrino Velocimeter does not measure the velocity of the water, but the velocity of the suspended particles the water body naturally contains. The four receivers of the Vectrino Velocimeter measure the three velocity components in x-, y- and z-direction which is relative to the probe (see Table 3.1). Because of the fourth receiver arm the vertical water velocity is measured twice and hence the z-velocity is measured with a lower uncertainty than the x-, or y-velocity and in addition a better representation of the turbulence can be ensured [9]. In Figure 3.4 the Vectrino Velocimeter which was used for the measurements is shown.

For getting an accurate representation of the velocity, the measurements are conducted at a sampling volume which is located 5 cm next to the transmitter to avoid any disturbances that could have a negative impact on the results.



(a) Instrument housing and probe head

(b) Probe head: Transmitter and the four receivers

Figure 3.4.: Vectrino Velocimeter with a side-looking probe

Before any measurements can be conducted the Vectrino software has to be installed on the PC. To ensure that the Velocimeter is activated the communication between the software and the instrument has to be checked. If everything works well the Vectrino Velocimeter can be configured. The following table shows all the parameters which were chosen:

Parameter	Chosen or default settings	Description
Sampling rate [Hz]	45	Define output rate for the velocity data
Nominal velocity range [m/s]	± 0.30	Covers the range of velocities during the data collection, set time shift of pulses to determine the Doppler shift
Sampling volume height [mm]	7.0	Default setting
Coordinate system	XYZ	Measurements transformed to a fixed orthogonal coordinates system
Power level	High	Transmitted acoustic energy of the instrument, difference to Low is 7 dB

Table 3.1.: Settings of the Vectrino Velocimeter

The model was run for both measuring instruments with a discharge of 92 l/s and with closed gates. The Vectrino Velocimeter was mounted on a tripod and was positioned above measuring points which were marked beforehand on selected cross-sections (see 3.3). All velocities were measured 5 cm below the water surface. Figure 3.5 shows the Vectrino Velocimeter mounted on a tripod.



Figure 3.5.: Positioning the Vectrino Velocimeter above a measuring point, photo: N. Olsen

Starting the velocity measurements is quite easy by activating the data collection. The velocities in all three directions are displayed on the computer. During each measurement or data collection the software is generating an ASCII file which can be imported into an Excel spreadsheet. For each measuring point the Vectrino Velocimeter measures approximately five minutes which equals to 13,500 samplings. For each point the average of the three velocities were computed. In Fig. 3.6 a characteristic velocity distribution is shown in one point.

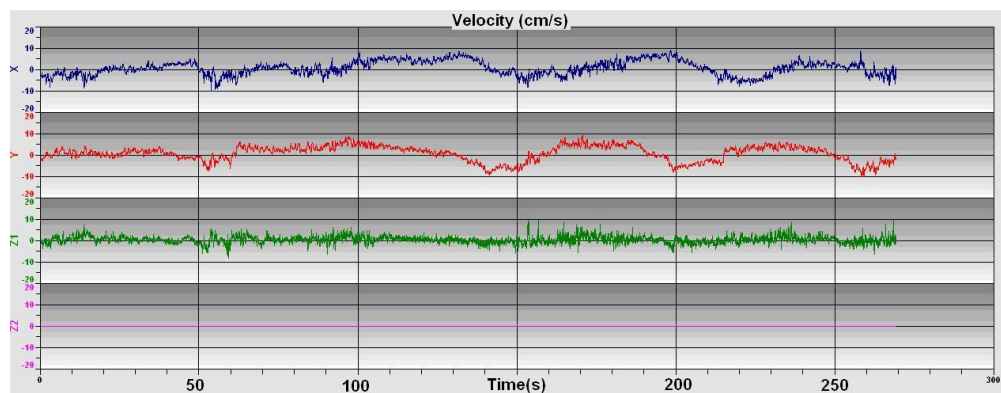


Figure 3.6.: Graphical view of the velocities at point 8 in cross-section 23

The velocities are fluctuating and there are two graphs for the vertical velocity. The Vectrino Velocimeter takes automatically the vertical velocity with the smallest standard deviation (Z1 in Fig. 3.6). The standard deviation is a parameter to quantify how much noise is accompanied with the measurements. Because the receiver pulse is sloped by an angle of 30° , the velocities which the Vectrino Velocimeter measures are consequently rotated by an angle of 15° [9]. The Vectrino software consists of a so-called probe check which can be used to control the quality of the measurements. The graph of the probe check shows how the signal alters with range and hence it can be observed where the measurements are taking place. A typical probe check is shown in Fig. 3.7:

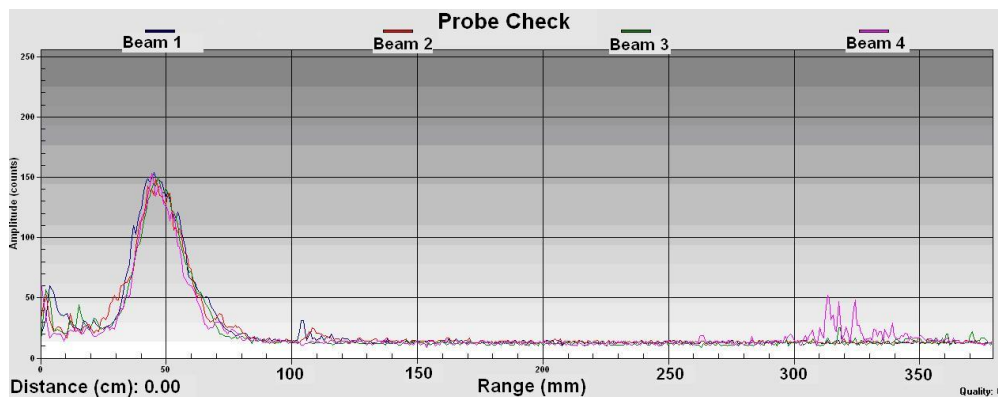


Figure 3.7.: Probe check of point 10 in cross-section 23

The individual lines illustrate the velocity components in the three directions. The beginning of the curve at the very left side shows the transmit pulse. The characteristic peak shows the area of the measurement volume and should be quite narrow. The small peak at approximately 105 mm represent the bottom echo.

In the following paragraph will be described how the measurements gathered by the Vectrino Velocimeter have to be manipulated so that the values can be compared with the values obtained by STAR-CCM+.

3.3. Evaluation of the measurements

All measurements are referred to the Origo (magenta point in Fig. 3.8) which lies upstream of the dam on the west side of the river. The coordinates and also the cross-section points were measured in the prototype and have to be scaled down to the model scale. As mentioned above the measuring points are all positioned on cross-sections. For determining the location and the coordinates of each point the distance from the Origo of the physical model to the first marked point of the cross-sections had to be measured. The distance measurement was conducted with a Laser distance reader which was pointed on a levelling staff. Besides, the distance from each point to the first point of the cross-section has to be measured. Displaying the cross-sections in AutoCAD is the easiest way to replicate the marked points from the physical model. Drawing circles with the distance as the radius, the first point (green points in Fig. 3.8) can be specified and the following points can be easily marked. AutoCAD provides the corresponding coordinates for each point in the three directions. Figure 3.8 shows the cross-sections including the measuring points where the measurements were conducted:

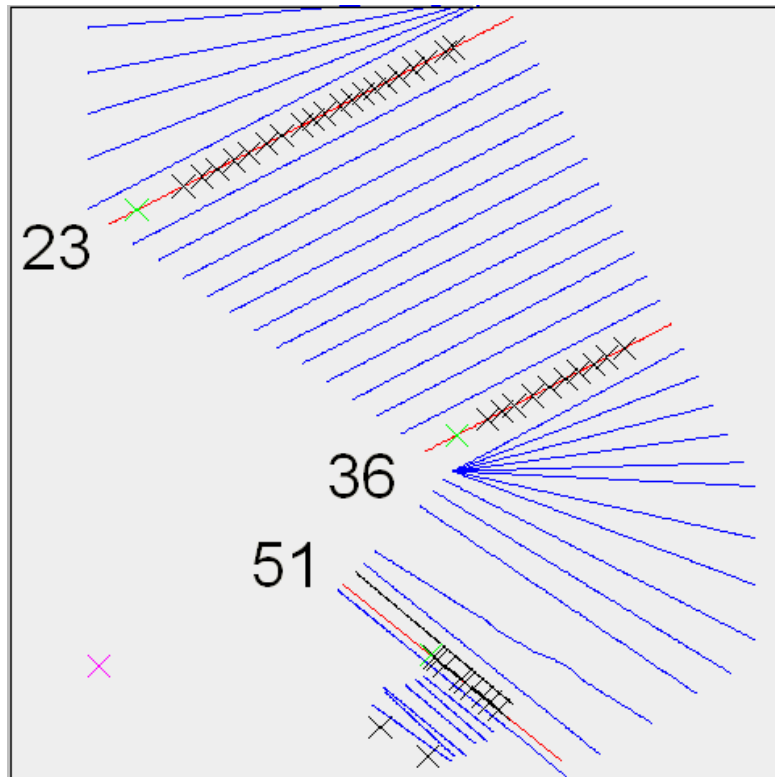


Figure 3.8.: Overview of the cross-sections and measuring points for the Vectrino measurements

The two points on the downstream end of the cross-sections are marking the position of the dam. Velocity measurements with the Vectrino Velocimeter were carried out at profile 23, 36 and 51. The profiles were chosen under the following aspects. The river regime shows some curves that implicate recirculation areas what are interesting flow pattern. Therefore profile 23 was chosen, where the recirculation area is existing on one end. Furthermore the cross-section is very wide and more measuring points could be specified. Profile 36 is further downstream and the river regime is more narrow with a higher water depth in the middle of the cross-section. The last cross-section should be close to the bridge pier to see how obstacles in water can influence the flow. Unlike the previous cross-sections, Profile 51 has to be constructed manually as a 2D line, because the profile in the physical model could not be found. Cross-section 23 and 36 are sloped at an angle of $\varphi = 27^\circ$. For cross-section 51 the angle is $\varphi = -39^\circ$. Figure 3.9 shows the coordinate system for the Vectrino Velocimeter which is relative to the probe.

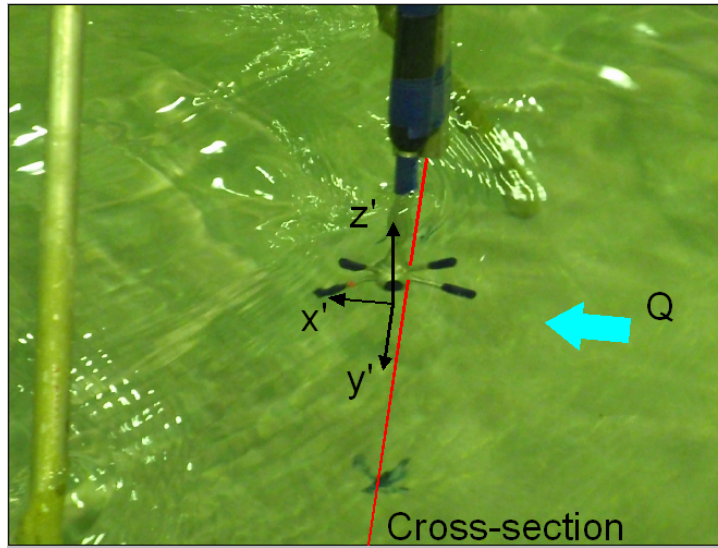


Figure 3.9.: Vectrino Velocimeter positioned above a measuring point along the cross-section showing the coordinate system

The x-direction is directed in flow direction, the y-axis shows along the cross-sections and the z-axis is towards the stem and represents the vertical velocity. For the velocities in x- and y-direction (u_{vv}, v_{vv}) a transformation is necessary to fit to the coordinate system in the laboratory. The vertical velocity obtained by the Vectrino Velocimeter is equal to the vertical velocity in the physical model. Hence, the u- and v-velocity have to be decomposed in respect to the coordinate system of the physical model. Figure 3.10 helps to find out which angle has to be taken.

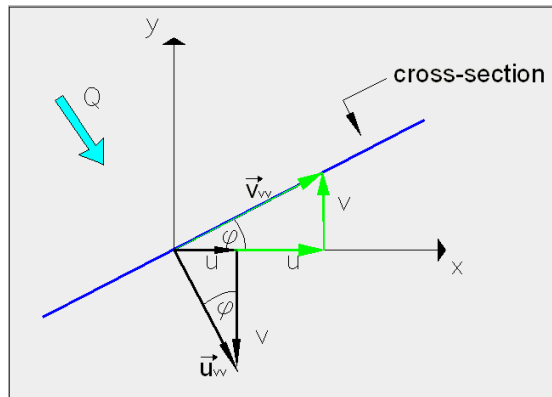


Figure 3.10.: Decomposition of the velocity along a cross-section

The velocities can be computed by the following equations:

$$\begin{aligned} u &= u_{vv} \sin \varphi + v_{vv} \cos \varphi \\ v &= -u_{vv} \cos \varphi + v_{vv} \sin \varphi \\ w &= w_{vv} \end{aligned} \quad (3.2)$$

u_{vv} is the x-velocity measured by the Vectrino, v_{vv} is the velocity in y-direction given by the Vectrino and φ is the angle of each cross-section. The vertical velocity w_{vv} measured by the instrument is equal to the velocities in the physical model.

3.4. Errors accompanying the measurements

The measurements with the Flow Meter were aligned for finding the maximum water velocity over the water depth of each point. This was quite difficult to achieve, especially because of the turbulent flow where the water direction was hard to define.

The measurements with the Vectrino Velocimeter were conducted 5 cm below the water surface. This is however, difficult to achieve, because the water surface is fluctuating. At the right side of profile 23 is the water surface mostly flat and no dominating underwater currents occur. These points can be measured more accurate than the points in secondary flow area. Furthermore, the tripod on which the Vectrino Velocimeter is mounted consists of three arms which are quite close to the instruments which might disturb the flow and influence the measurements. The measurements in profile 36 and 51 are both influenced by the irregular topography. The river bed has many bumps which are an obstacle for positioning the tripod right above the measuring point. Some points were located on a slope, so that the measuring instrument could not be positioned vertically. The water level was decreasing close to the boundaries where also points were marked. The side-looking probe is compared to the standard down-looking probe more suitable for shallow water. The measuring probe does not need a minimum distance to the river bed as long as the probe head is completely covered with water. Because the Vectrino Velocimeter conducts the measurements at the sampling volume which is positioned 5 cm next to the transmitter, the boundaries have an impact on the quality of the measurements. If the Vectrino Velocimeter is positioned too close to a boundary the transmitted pulse is not reflected by the particles in the sampling volume and the velocities can not be measured accurately. Besides the difficulties in hitting the right points, the transmitter of the Vectrino Velocimeter should be oriented along the cross-section. Because of the fluctuating water surface it is difficult to see down to the bottom where the points were marked.

It can be seen that measurements in the physical model are always accompanied with uncertainties on the conducting side and less from the instrument itself.

4. SHOCK WAVES

Shock waves are nothing else than ordinary waves, but propagating with a higher velocity. In the physical model shock waves were observed at two different places - in the stilling basin downstream of the spillway and between bridge and dam. The challenge of the measurements is that a physically correct copy of the shock waves is aspired.

In the following the general characteristics of shock waves will be explained and under which circumstances they occur. Furthermore, a description of the measurement will be mentioned with the results included.

4.1. Definition

Shock waves are generated by disturbances in supercritical flow. They occur on the free water surface and can be regarded as standing waves. Standing waves consist of either troughs or the more critical wave peaks [2]. Supercritical flows are characterized by the dimensionless Froude number above 1. It represents a very relevant number for gravity-driven flows in open-channel hydraulic and is defined as the ratio of inertia force to gravitational force:

$$Fr = \frac{v}{c} = \frac{v}{\sqrt{gA/B}} \quad (4.1)$$

v is the local velocity, c the wave propagation velocity, A the cross-sectional area, B the surface width and g the gravitational acceleration. In case the velocity v is smaller than the propagation velocity is $Fr < 1$, and the flow is subcritical. Is the velocity equal to the propagation velocity, then a critical condition is achieved and $Fr = 1$ [11]. When $Fr > 1$ the flow is supercritical and this type of flow is a hyperbolic problem that includes wave-type features. The shock waves disturb the continuous feature of the flow in terms of water depth and pressure distribution. Furthermore, the flow is sensitive for shock waves when obstacle, like piers, or changes in the geometry (change of direction, contraction or expansions) occur. The shock waves can be generated, because the channel upstream of the dam is more narrow than the reservoir. This contraction is similar to a funnel-shaped and is shown in Fig. 4.1.

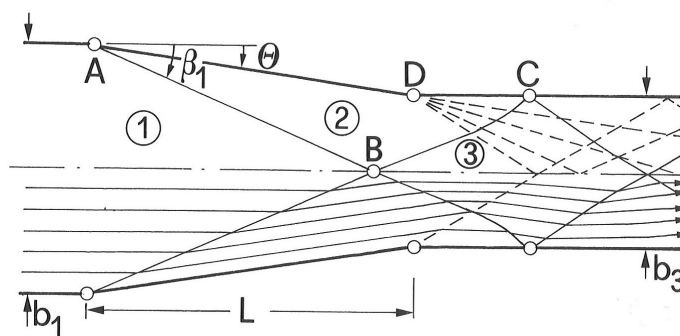


Figure 4.1.: Shock Waves in channel contraction, [2]

Figure 4.1 shows streamlines (long-drawn arrows) and shock waves which are marked with characteristic points. Region ① represents an uniform and undisturbed flow and is restricted by a wall with an arbitrary slope θ . Point A represent the starting point of the shock-waves which gets reflected on the opposite boundary below point C. This wave is a positive wave and is generated parallel to the negative waves which are characterized by point B. A positive wave leads to an increase of flow depth and the waves are generated abruptly. Negative waves however are specified by a decreased water depth and by a continuous wave forming. The superposition of both waves result in the characteristic feature of shock waves. The development of shock waves can be avoided, if the sidewall of region ① has a slope at an optimal angle θ . Consequently, the waves are propagating directly to point D and superposition leads to an undisturbed flow [2]. For the computation of shock waves either the exact or the depth-averaged Navier-Stokes equations are used. The latter is also called shallow water equations and includes non-hydrostatic pressure as well as momentum in the vertical direction. Both sets of equations yield fairly reasonable results for representing the wave peaks in the correct height and position compared to the measurements [12].

4.2. Measurements Of Shock Waves

Shock waves, as mentioned above, occur at two different location, but measurements are only carried out between bridge and dam. To capture the shock waves the water level was measured with a ruler which has to be positioned exactly vertical. To ensure this, a Laser, which was standing on the edge, was used. The Laser emits a vertical and a horizontal beam and when the ruler is parallel to the vertical beam, the heights could be read at the intersection point of the two beams. The measurements were conducted along the Laser light line. The area was divided by nine lines on which the measurements were conducted on 217 measuring points. For achieving a supercritical flow a high discharge was needed and the discharge was set to $892 \text{ m}^3/\text{s}$.

Supercritical flow also occur on a lower discharge, but at this discharge the complex pattern of the shock waves is more emphasized and hence the measurements can be conducted more easily. In addition to the high discharge the gates were completely opened to ensure a high velocity. The evaluation of the shock waves was done in Excel.

For analysing the water level the coordinates of the measuring points have to be specified, which was done in AutoCAD. In the physical model the cross-sections between the dam and the bridge were not visible. The Laser which were used for reading the correct water level from the ruler was also used for reproducing the cross-sections. Therefore, the measuring points were chosen

along the horizontal Laser line which was orientated parallel to the dam construction. For rebuilding the cross-sections in AutoCAD, one characteristic point of each side has to be marked on the edge of the model. From these points the distance to the Origo of the physical model was measured with a Laser distance reader. Additionally, another characteristic point, which position is known, was needed. The first point of cross-section 36 was used to calculate once more the distance to the two cross-section points. In AutoCAD, circles with the distance as the radius were constructed and the intersection point on each side of the river characterizes the cross-section. These points are the first points of the new created cross-section. Figure 4.2 shows the cross-sections and the measuring points:

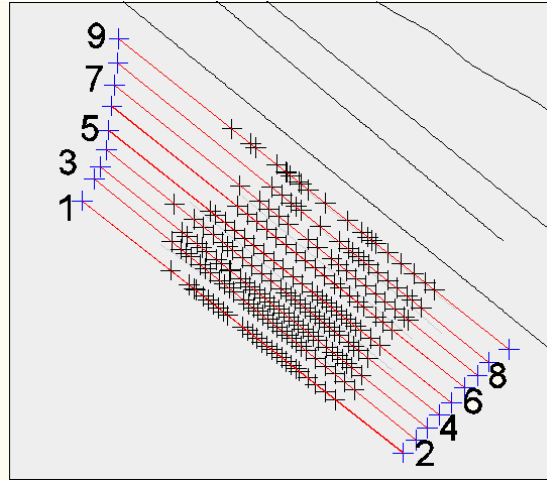


Figure 4.2.: Cross-sections and measuring points for the shock waves

Cross-section 9 is located close to the downstream side of the bridge pier and cross-section 1 is directly positioned on the upstream side of the dam construction. The green points represent the points where the measurements were carried out. The coordinates in x- and y-direction can be specified in AutoCAD and copied together with the appropriate water level in an Excel spreadsheet. Because the cross-section does not exist in the physical model, it was placed in AutoCAD in front of the bridge pier as a two-dimensional line only the x- and y-coordinates could be determined. The z-coordinates were determined by the two cross-sections upstream and downstream of the new cross-section. The distance between the horizontal Laser light and the water level was measured with a ruler. For measuring the position of the Laser light a needle, which is normally used to read the water depth, was used. The needle is adjusted that the zero point which is compatible to a reference value in the prototype. The reference value is 21 m a.s.l. The distance of the zero point and the horizontal Laser light was measured as $\Delta z = 0.407$ m. The coordinates of the cross-sections refer to the prototype and had to be manipulated in terms of the physical model. For the z-coordinates the cross-section values were increased by the provided factor of 54.

The equation for determining the correct values of the water level for each measuring point is consequently:

$$(21 + 54)/45 + 0.407 - h_{\text{gem}} \quad (4.2)$$

The factor 45 decreases the values to the model scale, h_{gem} are the values of the water level measured in the physical model displaced by the factor 2. The factor 2 has to be taken into account, because the whole geometry in AutoCAD was displaced in x-, y-, z-direction by the factors $\Delta x = 2$ m, $\Delta y = 6$ m, $\Delta z = 2$ m to avoid negative coordinates.

The water levels of all cross-sections were imported in form of an Excel spreadsheet into Tecplot

to produce a three-dimensional graphics of the shock waves. Figure 4.3 depicts the shock waves occurring in the physical model and the measured shock waves plotted with Tecplot.

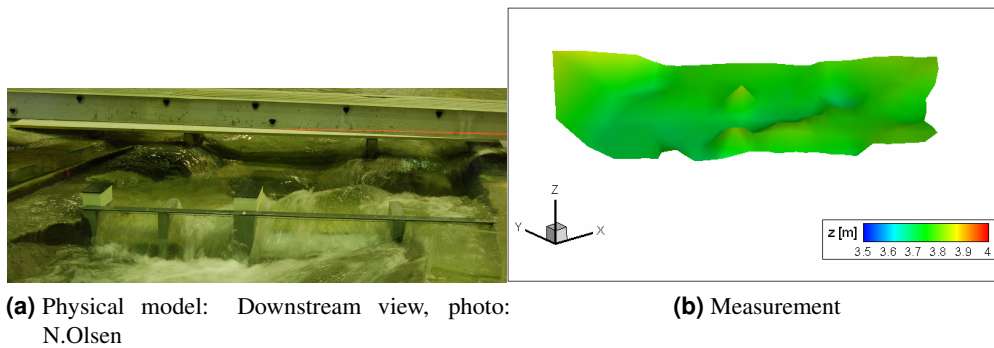


Figure 4.3.: Overview of observed and measured shock waves

The shock waves in front of the Figure 4.3 (a) occur on the downstream side of the dam and were not measured. The measured shock waves are in the middle of the Figure 4.3 (a) upstream of the dam construction. The figure shows also the horizontal Laser light which defines one of the cross-sections.

The measurements were accompanied with some uncertainties accompanied by reading the correct height of the water level. The shock waves were not stationary and were oscillating in flow direction. Furthermore, the ruler has to be positioned correctly vertical which was not always easy to achieve. For ensuring undisturbed measurements a bridge (see Fig. 4.3 (a)) was put over the reservoir from which the measurements could be conducted.

5. NUMERICAL MODEL

5.1. Introduction to Turbulence

Turbulence is an ubiquitous phenomena and can be described by a lot of different characteristics, but a general definition does not exist. The velocity field of turbulent flows is three-dimensional, time-dependent and have a random and irregular feature. Furthermore it consists of a complex motion influenced by vortices which can always occur even if the flow is irrotational. The vortices consist of different sizes-from the largest size depending on the geometry to the smallest which gets destroyed by viscous processes. These viscous processes are responsible for the dissipative feature of turbulence [13]. In 1922, Richardson found out that the largest scales get kinetic energy out of the main flow and this energy is transferred to smaller scales until the energy is dissipated by viscous processes. This is called the energy cascade and it is an important process in turbulent flows. It takes care that energy gets dissipated at the smallest scales, which occurs at the Kolmogorov's scale. The first person who give the turbulence a number was Reynolds. In experiments he found out that the transition from laminar to turbulent in a pipe occurs by an Reynolds number of approximately 2000 and in open channel flows at around 500. The Reynolds number is defined as the ratio of inertia forces to viscous forces:

$$\text{Re} = \frac{UD}{\nu} \quad (5.1)$$

The Reynolds number consists of a characteristic velocity, length and kinematic viscosity. Re plays a crucial role in the distribution of the scales. With increasing Re the scales become finer and vice versa.

5.2. Computational Fluid Dynamic

Most of the fluid dynamics are described by non-linear, partial differential equations which are with few exceptions analytical not solvable. An example are the Navier-Stokes Equations (5.3). These equations describe the flow of fluids (laminar and turbulent) and it is still an enormous incentive to find a global solution. The Navier-Stokes Equations are an important part of CFD which deals with the solution of the equation that occurs from the approximation method. The differential equations are solved on the basis of the discretization method. This method solve the equations approximately with several algebraic equations and the continuous solution field is replaced by a finite one. That means that the physical procedures are described on discrete positions [14]. In the last few years a considerable progress has been achieved in the field of CFD which is linked to the development of faster computers. Another influence of the computational time, simulation cost, efficiency and stability of the results are the different approaches which can be used to compute turbulent flows. There exists three main approaches for turbulent flows:

1. Direct Numerical Simulation (DNS)
2. Large Eddy Simulation (LES)

3. Reynolds-Averaged Navier-Stokes (RANS)

The **DNS** solves the Navier-Stokes Equations by resolving all the scales of motion. This is only possible if a very fine grid is used to resolve even the smallest eddies. This procedure is very extensive and has enormous computational requirements but gives the best accuracy. Furthermore only fluid flows with small Reynolds numbers can be considered, because the grid has to be finer with increasing Reynolds numbers.

LES is based on the separation of the computed and modelled structures. The large eddies are computed explicitly and the small scales are modelled. Because of the simulation of only the larger eddies the grid can be coarser, the simulation costs are lower and the modeling complexity increases in respect to DNS.

RANS represents a statistical view of turbulence. The Navier-Stokes Equations are time-averaged and therefore only steady equations for the mean values have to be solved. But the fluctuations caused by the turbulence still appears in the equations as an additional term, the so-called Reynolds-stress term. The RANS equations only differs from the Navier-Stokes equations by the Reynolds-stress term which inserts six more unknowns. Because of the averaging process a closure problem occurs and to be able to solve these equations the Turbulence Model was determined. More about the Turbulence Model can be read in 5.5. The disadvantage of RANS is that it is difficult to get an universal model, because the fluctuations are strongly influenced by the geometry. In comparison with the other two approaches is RANS the one with the greatest modeling complexity, but with the lowest accuracy.

5.3. Navier-Stokes Equation

The Navier-Stokes equation are named after Claude Louis Henri Marie Navier and Sir George Gabriel Stokes and consists of the continuity and the momentum equation.

$$\nabla \mathbf{u} = 0 \quad (5.2)$$

$$\delta_t u_i + u_j u_{i,j} + \frac{1}{\rho} p_{,i} = \nu u_{i,jj} \quad (5.3)$$

The equations are written in tensor notation. This notation means that terms with repeating indices are summed up over the three values of the index [13]. The left side of the momentum equations consist of three terms. The first term is the transient term and can only be neglected when steady flow is regarded. The next term describes the convection processes and is nonlinear. The last term on the left side is the pressure term and the term on the right side includes the viscosity and is known as the diffusive term. These equations represent a three-dimensional, time-dependent and incompressible flow and are restricted to Newtonian fluids. For the derivation an infinitesimal control volume is regarded. For each control surface are the momentum fluxes, shear- and normal stresses, pressure and gravitational forces defined. The momentum equations are derived from Newton's second law under the assumption of mass conservation. These four equations describe the flow and pressure field accurately by using the appropriate initial and boundary conditions. Moreover, the equations are 2nd-order differential equation and nonlinear. Solving these equation accurately is not possible, because the smallest scales correspond with the dimension of about 1/1000 of the flow area. To ensure that no information

are getting lost the area has to be resolved by a mesh of the size $1000 \times 1000 \times 1000$ mesh points. With the existing computers, even with supercomputers, is it not possible to solve the exact Navier-Stokes equations. For using these equations the most common approach is to average the Navier-Stokes equations with respect to time which will be described in the following paragraph (5.4).

5.4. RANS

For the derivation of the RANS equations, the velocity field has to be decomposed in a mean and fluctuation part [15]:

$$\mathbf{u}(\mathbf{x}, t) = \langle \mathbf{u}(\mathbf{x}, t) \rangle + \mathbf{u}'(\mathbf{x}, t) \quad (5.4)$$

This treatment is called Reynolds decomposition and substituting it into the momentum equations and after averaging the equations with respect to time the averaged momentum equation or RANS equation are derived:

$$\langle u_i \rangle_{,i} = 0 \quad (5.5)$$

$$\delta_t \langle u_i \rangle + (\langle u_i \rangle \langle u_j \rangle)_{,j} + \frac{1}{\rho} \langle p \rangle_{,i} = \nu \langle u_i \rangle_{,jj} - \langle u'_i u'_j \rangle_{,j} \quad (5.6)$$

The last term on the right side is the Reynolds-stress term, which is responsible for the closure problem of RANS equations [15]. The stress term is a symmetric second-order tensor:

$$\langle u'_i u'_j \rangle = \langle u'_j u'_i \rangle \quad (5.7)$$

This term occurs because of the momentum transfer caused by the fluctuations in the velocity field. The diagonal components are the normal stresses, the off-diagonal are the shear stresses. Because of the symmetry the tensor reduces from nine to six unknowns. These unknowns have to be determined with a Turbulence Model, because an explicit calculation is not possible. The next chapter introduces the theory of these models (5.5).

5.5. Turbulence Model

The term Turbulence Model represents a set of equations for determining the Re-stress term. The most successful closure in RANS modelling is the turbulent viscosity model. It is based on Boussinesq's hypothesis and the following procedure shows how the equation for the Reynolds-stress can be defined. First the turbulent kinetic energy (TKE), which is half the trace of the Re-stress tensor has to be introduced:

$$k = \frac{1}{2} \langle u'_i u'_i \rangle \quad (5.8)$$

The Re-stress can be expressed as:

$$\langle u'_i u'_j \rangle = \underbrace{a_{ij}}_{\text{anisotropy}} + \underbrace{\frac{2}{3} k \delta_{ij}}_{\text{isotropy}} \quad (5.9)$$

Where δ_{ij} denotes the Kronecker delta. The anisotropy tensor a_{ij} is defined by the mean velocity gradient:

$$\begin{aligned} a_{ij} &= -\nu_t \left(\frac{\delta \langle u_i \rangle}{\delta x_j} + \frac{\delta \langle u_j \rangle}{\delta x_i} \right) \\ &= -2\nu_t \bar{S}_{ij} \end{aligned} \quad (5.10)$$

\bar{S}_{ij} is the rate-of-strain tensor and ν_t stands for the turbulent viscosity, also known as the eddy viscosity. The formulas show that Boussinesq assumed that the anisotropy tensor a_{ij} is aligned with the mean-rate-of-strain tensor. Furthermore the hypothesis is based on the assumption that the anisotropy is determined by the local mean-rate-of-strain \bar{S}_{ij} . Experiments shows that both assumptions are incorrect, especially for complex flows [16]. The challenge now is to determine the turbulent viscosity. There exists different approaches like the mixing length model, introduced by Prandtl (1925). The turbulent viscosity consists of two parameters, the mixing length and the velocity scale. It solves the RANS equations in addition to algebraic expressions. However, for each flow case the parameters have to be adjusted.

A better approach is the one-equation model including the k-model and the Spalart-Allmaras model. The k-model uses the turbulent kinetic energy and also the mixing length to define the turbulent viscosity. The kinetic energy is determined by a transport equation, which will be shown later, and the mixing length still has to be specified. Both the mixing length and the k-equation are based on the turbulent viscosity and therefore a poor replication of the turbulence has to be taken into account.

The Spalart-Allmaras model is not using the mixing length. It consists of a convection-diffusion equation plus a source term, including e.g. a mean flow rotation and a destruction term. The Spalart-Allmaras model is tested in the fields of aerodynamic and shows a pretty good prediction of the turbulence, but still a more advanced model is necessary [15].

The most common model available in CFD programs is the k- ϵ model. The model is based on the Boussinesq hypothesis for the Re-stress term. The formula for the turbulent viscosity consists of two turbulent scales, k and ϵ :

$$\nu_t = C_\mu k^2 / \epsilon \quad (5.11)$$

$C_\mu = 0.09$. Besides this coefficient four more are used in this model. Furthermore two transport equations are inserted for the both scales. The k-equation (same as in the one-equation model) is defined as:

$$\frac{\overline{Dk}}{\overline{Dt}} - P = \nabla \cdot \left(\left(\nu + \frac{\nu_t}{\sigma_k} \right) \nabla k \right) - \epsilon \quad (5.12)$$

With the turbulent Prandtl number $\sigma_k = 1$. The transient and convective term are mostly expressed using the Lagrangian derivative, in this case the average has to be regarded, and is defined as: $\frac{\overline{D}}{\overline{Dt}} = \frac{\partial}{\partial t} + \langle u \rangle \nabla$. The production term is a source term and is defined as

$P = -\langle u'_i u'_j \rangle \langle u_i \rangle_{,j}$. The term is mostly positive and has a crucial part in the equation. ϵ is the dissipation rate, which includes the mixing length. The terms on the left side are known, but the terms on the right side are unclosed. For ϵ an modeled equation is used even an exact equation could be derived from the Navier-Stokes equation, but it is unfeasible to get a solution.

$$\frac{\overline{D\epsilon}}{\overline{Dt}} = \nabla \cdot \left(\frac{\nu_t}{\sigma_\epsilon} \nabla \epsilon \right) + C_{\epsilon 1} \frac{P\epsilon}{k} - C_{\epsilon 2} \frac{\epsilon^2}{k} \quad (5.13)$$

With coefficients: $\sigma_\epsilon = 1.3$, $C_{\epsilon 1} = 1.44$, $C_{\epsilon 2} = 1.92$. The term on the left side is the convection term, the first term on the right side is the diffusion followed by the production and destruction term.

Consequently, the k - and ϵ -term as well as the convective term are expressed as differential equations. The modelled quantities are the Re-stress term and $\overline{D\epsilon}/\overline{Dt}$. The k - ϵ model includes still the turbulent-viscosity hypothesis and because of that the model is not sufficient for complex flows. To get more accurate results the coefficients could be adjusted, e.g. C_μ which is only a roughly guessed value and is actually depending on the Reynolds number.

STAR-CCM+ offers four turbulence models. The above mentioned Spalart-Allmaras and k - ϵ model and in addition the k - ω model and the Reynold stress turbulence. The basic idea behind the k - ω model is very similar to the k - ϵ model and only differs in the way of determining the transport equation for the second scale. ω represents the characteristic frequency of large scales and is defined as the ratio of the dissipation ϵ to kinetic energy k . The advantages over the k - ϵ model is the better approach of flows close to walls. The last model which will be mentioned is the Reynolds - stress transport model. This model is not based on the turbulent viscosity hypothesis and the determination of the transport equation for the Re stress term is derived from the Navier-Stokes equations.

5.6. Discretization Scheme

For the discretization it can distinguish between spatial and temporal discretization. There exists several spatial discretization schemes. The most known are the Finite-Difference, Finite-Element and Finite-Volume approach. Because STAR-CCM+ is based on the Finite-Volume method only this method will explained further.

The Finite-Volume method introduces a finite control volume (CV). The method is based on the conservation law. That means, that mass and momentum flowing into the control volume also has to flow out. This corresponds to an equilibrium state which excludes all kind of source and sink terms. The solution domain is replaced by a finite amount of control volumes and for each CV the conservation equations have to be fulfilled [17]. The Finite-Volume method always fulfills the total balance of mass, momentum and energy. The center of each CV is a calculation node on which all the boundary values are referred to by interpolation. That means, that each CV gets an algebraic equation including the neighbour nodes. The advantages of this method is that it is convenient for complex geometries [17].

Temporal Discretization is required for parabolic problems - thus for time-dependent flows. The transient term will be determined at a new point of time t_{n+1} by using the current time level t_n as a known value [14].

$$\left. \frac{\partial \phi}{\partial t} \right|_{t_{n+1}} = \frac{\phi_i^{n+1} - \phi_i^n}{\Delta t} \quad (5.14)$$

ϕ is the solution of the differential equation, Δt is the time-step and i represents the grid points. ϕ_i^{n+1} is the unknown term and in order to solve this equation the appropriate equations for the other points also have to be taken into account ($i = 1, N$). Because of solving several equations the solution process is very complex. But the method, which is also known as Euler Implicit, is more stable than e.g. explicit method. STAR-CCM+ also offers the second-order temporal discretization method, which will not further explained.

5.7. VOF

VOF is an acronym for Volume Of Fluid and is one of the methods which can be used to determine the water surface. A flow which consists of two immiscible phases, in this case air and water, is called a multi-phase flow. With the VOF model, the location and shape of the interface, also known as the free surface, can be determined. The water body is discretized by cells and the main principle is to compute the fraction of water in each cell at a given time. In order to compute such a distribution a transport equation for the volume fraction has to be solved [18]:

$$\frac{d}{dt} \int_V \alpha_i dV + \int_S \alpha_i (\nu - \nu_g) \cdot da = \int_V s_{\alpha_i} dV \quad (5.15)$$

The first term represents the transient term, followed by the convective term, $\alpha_i = \frac{V_i}{V}$ stands for the volume fraction and s_{α_i} describes the source or sink term.

5.8. Characteristics of Numerical Methods

The main characteristic of a numerical simulation is the convergence. For achieving convergence two characteristics have to be fulfilled - consistence and stability. Because the solution domain is divided into cells or control volumes the variables are calculated as approximate values. The difference between the exact differential equation to the discretization of the exact differential equation by approximation is known as truncation error. If this error strive to zero the method satisfies the consistence. For getting a stable solution the occurring error should not increase during a simulation. Satisfying the stability is difficult to achieve when boundary conditions and non-linearity are part of the simulation. A solution is converging as long as the solution of the exact differential equation is close to the approximate differential equation [17]. Non-linear equations are solved iteratively. An unknown variable is computed by guessing the other unknown. The iterative method ensure an improved solution which can be used to continue with the calculation. This procedure will be repeated until a converged solution is obtained [17]. For computing the value at a new iteration step (i) a relaxation factor can be used instead of using the total value from the previous iteration (i-1). A new variable, named v, can be computed with the following equation:

$$v = r \cdot v_i + (1 - r) \cdot v_{i-1} \quad (5.16)$$

where r is the relaxation coefficient and should be in the range of 0 and 1 [3]. The task of a relaxation factor is to eliminate the fluctuations in the values of previous iteration to smoothen the values for the new iteration. The converging process takes much longer by applying a relaxation factor. By decreasing the value the solution becomes more stable and divergence can be limited.

5.9. Source of Errors and Uncertainties

The numerical solutions are only approximated solutions which leads to several systematic errors. The following list gives an overview of the errors including their description:

1. Modelling error:

A modelling error is the difference between the real flow and the exact solution of a model based on mathematical equations. For turbulent flows this error has to be considered of which introduces that even the exact solution of the numerical model is not representing the reality totally. Modelling errors also occur when the examined geometry is simplified by boundary conditions [17].

Another source for modelling errors is the $k - \epsilon$ turbulence model. The turbulence model is based on the theory of an isotropic turbulent viscosity even if non-isotropic conditions occur [3].

2. Discretization error:

The discretization error is known as the difference between the exact solution of the differential equation and the exact solution of the approximated solutions [17]. The error can be reduced by applying a finer mesh. Additionally, the order of the approximation process has influences on the accuracy. First-order schemes might lead to problems in respect of false diffusion [3].

3. Iterative error:

Iterative errors describe the difference between the exact solution of the approximated equation and the solution obtained by the iterative process. The error is also known as the convergence error. Convergence is quite difficult to achieve and depends on different factor like time-step, mesh type or iteration step. If convergence is not obtain the solution can lead to inaccuracies [17].

4. Round-off error:

The round-off error is based on the inaccuracies of processors of the computer. This error is for nowadays computers (mostly using 64 bits floating point numbers) extremely small and can be neglected [3].

5. Uncertainties in input data and boundary conditions:

These errors are difficult to avoid and exist in every simulation. To avoid these errors the mesh has to fit to the water level and river bed completely. The velocity for the inflow boundary conditions might also cause errors [3].

6. Bugs in the software:

CFD program are never free of bugs and there are mostly hidden and difficult to evaluate [3]. The software tends to crash during a runs.

7. Human errors due to inexperience:

Human error are natural. The world of each CFD program is very complex. Choosing the wrong parameters or algorithmen can cause a tremendous error.

6. SOFTWARE

This chapter gives an overview of the different software which was used for the numerical study. Moreover, a deeper introduction of the commercial program STAR-CCM+ is given. It starts with some general information about the program and leads over to the description of setting up the simulation using the essential parameters. The development of computer programs is an improvement for analyzing systems which are in the theoretical handling too complicated. In this thesis two programs have been mainly used, the three-dimensional CFD program STAR-CCM+ and the computer aided design, AutoCAD 2010, software for creating 3D drawings. In the two following paragraphs the usage of these programs is described more deeply. Besides these programs, Microsoft Excel was used for handling all the data from the Vectrino Velocimeter and from the measuring of the shock waves. For visualizing the shock waves the visualization software Tecplot 360, version 2009, was used. With that software, three-dimensional views can be produced by importing the required data as an ASCII file.

6.1. AutoCAD

In order to get good results it is important to replicate the geometry of the physical model accurately. AutoCAD 2010 is a product of Autodesk and is used for this thesis to create 3D drawings. With the program the user has the ability to export the drawings in STL format, which stands for stereo lithography. This is one of the formats which STAR-CCM+ supports.

With AutoCAD, the reservoir including the dam and bridge pier was designed as a 3D solid. The reservoir bed was constructed using the provided data of the cross-sections. These values had to be adjusted to the Origo and the physical model. The manipulated values were used for constructing the geometry in AutoCAD. For the dimensions of the dam the heights, length and width of the gates, dam pier and bridge pier was measured in the physical model. Hence, all coordinates and dimension are referred to the model scale.

Because of the large length of the river the total number of the cross-sections was divided into four parts. For each part a box had to be created in which the water can flow. The box consists of two parts - the perimeter and the river bed. For constructing the perimeter the z-coordinates of the cross-sections were set to zero and afterwards imported into AutoCAD. The outer points were connected with a polyline which was extruded to 3 m. The surface of the river bed was created as a 3D Loft by using the space between each cross-section. After the perimeter and the 3D surface were created, the two parts were copied together. Because the surface should represent the river bed the design has to be sliced. Consequently the surface represents the river bed and has vertical side walls of 3 m height. This was performed for each part and afterwards, those were connected to produce the whole river geometry. Figure 6.1 shows the individual steps of one part to construct the geometry.

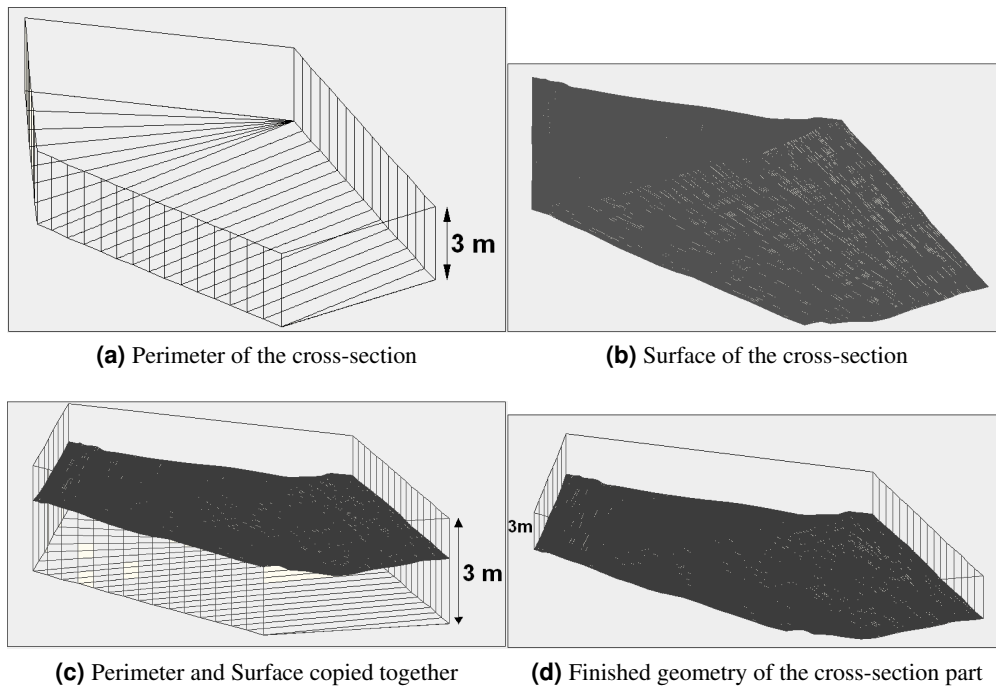


Figure 6.1.: Example: Creating the geometry for STAR-CCM+ on one part of the cross-sections

The dam was designed separately and combined with the cross-sections afterwards. The dam construction and the bridge pier has to be subtracted from the modified cross-sections to get a complete geometry. The finished geometry revealed that the right bridge pier is positioned on the side and has no influence on the flow.

Before the STL file could be created the finished geometry had to be shifted because the downstream part of geometry had negative values. AutoCAD 2010 only generates a STL file for positive values and is shifting the geometry automatically in a positive region. The values of that displacement is however unknown. Because all the coordinates have to be adjusted for comparing the measuring values with the simulation values accurately it is important to know the position of the geometry exactly. Therefore the whole geometry was displaced in x-, y- and z-direction. The components for the simulation with closed gates were set to $\Delta x = 1$ m, $\Delta y = 3$ m and $\Delta z = 1$ m. Because the measurements were taken for two different positions of the gates, two STL files had to be generated with the appropriate position of the dam construction. For the velocity measurements the gates were closed whereas for the shock waves a open gate position was chosen.

6.2. STAR-CCM+

STAR-CCM+ was developed by CD-adapco and version 4.06.011 was used in this thesis. It is a general-purpose CFD solver which uses the Finite-Volume method and handles structured and unstructured grids. Furthermore, STAR-CCM+ supports several turbulence and multiphase models. The software is divided into a client and a server. The client is based on Java and handles the user interface. The function of the server is to carry out the computing operations [19]. The simulation commands (like importing data or running the simulation) are performed on the server, which was controlled by a Laptop over a Remote Desktop Connection.

6.2.1. General features

The graphical user interface consists of a simulation window, which is built up like a tree. It contains nodes that direct the user to the different objects of the simulation. These objects navigate from the more seizable concepts like regions to the less evident material properties. For changing or controlling the coefficients the Properties Window exist. The simulation window manages all the objects needed for the simulation. One of the objects is the continua which is generated automatically during the import of the geometry. The Continua contains the meshing as well as the Physics Models and also the Initial Conditions and Reference Values. Not part of the continua, but associated to it is the next object called Region. The region contains all the boundaries of the geometry with the corresponding Physics Values, Mesh and Physics Conditions (depending on the meshing model).

6.2.2. Pre-Processing

This paragraph consists of the determination of the different boundaries and the mesh generation. The terms Field Function and models will be introduced. An overview of the selected Physics Models is given in Table 6.5. Moreover, the principle of the Volume of Fluid and the Finite-Volume method will be explained further.

After importing the STL file, the whole geometry is one region and has to be divided into its boundaries to separate between solid, fluid and porous surfaces. The program includes different types of boundaries. The following Table gives an overview of the boundary types used in the simulation:

Type	Description	Name in simulation
Velocity Inlet	First cross-section; velocity as Field Function	Inflow
Pressure Outlet	Last cross-section and bottom downstream of dam; static pressure is specified	Outflow and Outlet
Wall	Side walls, river-bed, dam and bridge pier; impermeable surface	Wall, Bottom, Dam, Pier
Symmetry	Top Surface; imaginary plane on which the mesh is mirrored	Top

Table 6.1.: Boundary types used in the simulation

The bottom downstream of the dam is defined as a pressure outlet to ensure that the passing water has no influence on the flow over the dam.

For each boundary type the Physics Conditions and Physics Values are different. Table 6.2 gives an overview of the Physics Conditions, selected methods and the methods which could have been used instead. The Table rely on the simulation of the Sarpfossen dam and differs for other simulations.

Boundary type	Physics Conditions	Selected Method	Alternative Methods
Inflow	Flow Direction Specification	Boundary-Normal	Components, Angles
	Turbulence Specification	Intensity+Viscosity Ratio	K+epsilon, Intensity+Length Scale
	Velocity Specification	Magnitude+Direction	Components
Bottom	Shear Stress Specification	No-Slip	Slip
	Tangential Velocity Specification	None	(Local) Rotation Rate, Vector
	Wall Surface Specification	Rough	Smooth
Outflow	Backflow Direction Specification	Boundary-Normal	Extrapolated
	Target Mass Flow Option	nothing specified	nothing specified
	Turbulence Specification	Intensity+Viscosity Ratio	K+epsilon, Intensity+Length Scale

Table 6.2.: Physics Conditions of each boundary type

The remaining boundary types, dam, pier and wall, are equal to the bottom conditions except the method of the Wall Surface Specification is defined as smooth. The top boundary has no Physics Conditions node.

The Physics Values nodes is similar for each boundary type, but differs for the outflow and inflow boundary. Because the wall surface of the bottom boundary is set to rough the roughness height can be specified in the Physics Values node [18]. For both simulation a roughness height of 2 mm was defined and correspond to the roughness of a good-quality concrete.

For the outflow and inflow boundary the Turbulent Intensity is set to the default value of 0.01 and the Turbulent Viscosity ratio to 10. The value for the Turbulent Intensity is the lowest limit and should not exceed the upper limit of $I = 0.1$. The Turbulent Viscosity ratio is defined as the ratio of the turbulent viscosity to the dynamic viscosity μ_t/μ , and is used, if no turbulent lengthscale can be specified [18]. The latter is a molecular quantity and is responsible for the dissipation of the turbulence. For the initial condition this ratio was set to the upper limit of 100, because the inflow was quite turbulent and this number means that 100% of the initial velocity are turbulent fluctuations.

Furthermore, both boundary types contain of the Volume Fraction node which expresses the spatial distribution of the two phases, water and air. [18] The method for the outflow is set to zero. However for the inflow, the Volume Fraction relies to the composite method, which specifies the distribution of the water (H₂O) and air phase separately. For the H₂O node a so-called Field Function was defined, because a constant value was not satisfying the inflow condition. Also for the velocity magnitude was a Field Function defined. Field Functions are non-standard functions and are mostly used for non-uniform flows [18]. The following Field Functions were used:

$$(\$Position[2] < = z_s)?v : 0 \quad (6.1)$$

$$(\$Position[2] < = z_s)?1 : 0 \quad (6.2)$$

The Field Function is comparable to an if statement in programming language. If the condition (in the round bracket) is satisfied, then a special value is valid, else the other value will be taken. z_s represents the z-component. The water depth in the physical model was measured with a stationary needle (h_{model}). The variable z_s is the height of the water level increased by the displacement factor $\Delta x = 1$. The velocity v represents the velocity at the inflow. An overview of the values for the two different positions of the gate openings is given in Table 6.2b.

In the simulation the first equation is called Initial Distribution. It represents the Field Function for the velocity profile and is included in the velocity magnitude term for the inflow boundary. Equation 6.2 was used for the Volume Fraction of H₂O.

Variable	Closed gates	Open gates
h_{model} [m]	1.8185	1.88
z_s [m]	2.8185	2.88
v [m/s]	0.187	0.341

Table 6.3.: Values for the Field Function for closed and open gate position

Figure 6.2 shows the water surface by using the Volume Fraction of H₂O. The surface represents the cells which are half filled with water and air.

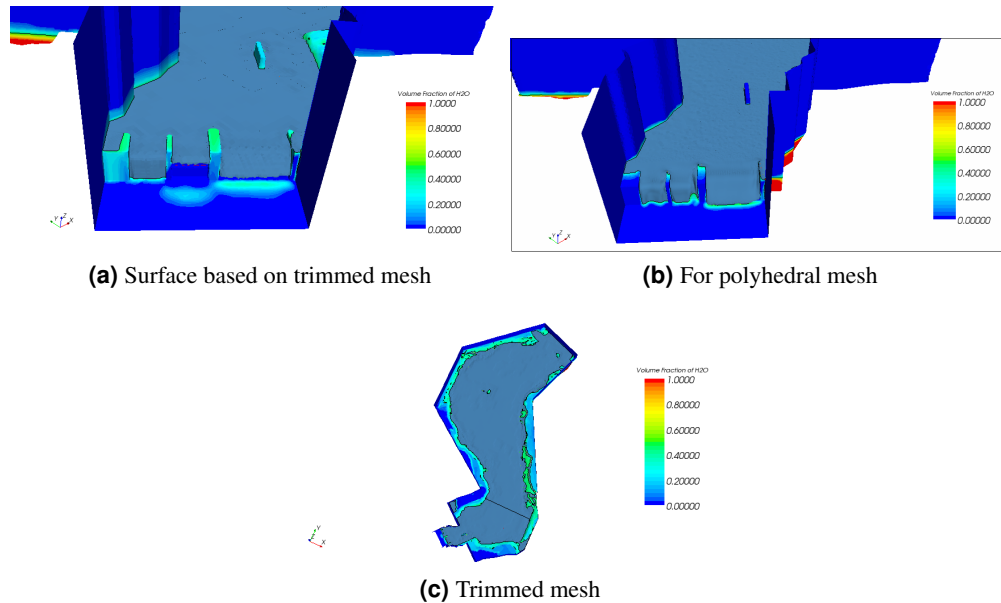


Figure 6.2.: Scalar scene: Overflow over dam by applying the Volume Fraction of H₂O ((a)-(b)), Reservoir ((c))

For generating a mesh, STAR-CCM+ distinguishes between a surface and a volume mesh. The latter will be used for the simulation. Both meshes can be produced separately and there are two ways of setting up these meshes. It is possible to make a surface mesh with AutoCAD and import it as a STL format to STAR-CCM+, where the volume mesh can be created. In this thesis however, the entire mesh was generated in STAR-CCM+ and the geometry, which was constructed in AutoCAD and converted to a STL format, was imported as a surface mesh into STAR-CCM+. For getting an optimal volume mesh the following criteria for the surface mesh should be adhered. It should be closed, manifold, not-intersecting and triangulated. Moreover

should all triangles be equilateral and the mesh sizes of neighbouring cells should vary continuously. These requirements are necessary for multi-regions to ensure a continuous surface [18]. Because the STL format imports the surface with a minimum amount of triangles the quality is mostly poor. For improving the surface quality a Surface Remesher or a Surface Wrapper can be used. The quality of the mesh has a crucial influence in the convergence. It also effects the Finite-Volume approach in terms of the accuracy. For creating the volume mesh it can be selected between trimmed, tetrahedral, thin or polyhedral cell types. Trimmed cells are mostly hexahedral cells with a high robustness and quality (Fig. 6.3 (a)). Close to the dam and bridge pier the mesh will be automatically refined. The trimmed cells are the only meshes STAR-CCM+ supports which are based on an orthogonal mesh. A tetrahedral mesh uses in comparison to the other volume mesh types the minimum amount of memory and is also fastest in mesh generation (Fig. 6.3 (b)). For thin geometries, the thin mesher is the best choice of the available volume mesher. It contains of prismatic cell shapes which are mostly applied for thin flat parts. Because the thin mesher uses either tetrahedral or polyhedral cells for the non-thin parts of the geometry a fewer amount of cells are required. Also the polyhedral mesh type uses fewer cells compared to a tetrahedral mesh and is in addition easily to construct. Polyhedral meshes are built upon the automatically generated tetrahedral mesh [18].

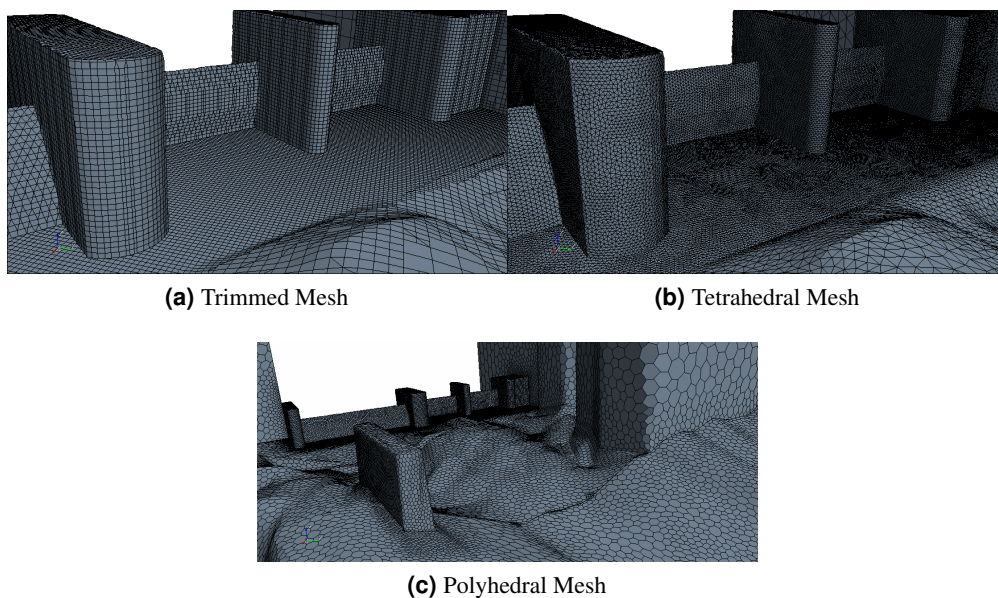


Figure 6.3.: Different mesh types

The following mesh types were chosen for the simulation:

Mesh Types	
Surface Mesh	Surface Remesher
Volume Mesh	Polyhedral Mesher

Table 6.4.: Selected Meshing Models

A Polyhedral Mesh (Fig. 6.3 (c)) has the advantage that the mesh is getting finer automatically close to geometries, like dam and bridge pier, and is hence well-suited for complex geometries.

All volume mesh types, except of the thin mesher, have a volumetric control integrated which is able to change the mesh density locally and is also known as nested mesh. In advance a volume shape has to be generated where refinements are required. For the volume shape either a block, cylinder, cone or sphere can be chosen, but also combinations are allowed [18]. The size of the cells can be chosen as a relative value to the base size of the coarse mesh or as an absolute value. The value for the relative size is given in percentage. For constructing a nested mesh it is useful to define an own coordinate system on a suitable point of the geometry. The advantage is that the dimensions of the volume shapes (length, width and height) can be specified more easily.

For generating the solution some essential variables and properties, like flow regime, solver type, fluid, kind of motion and mathematical formulations (k- ϵ model) have to be defined to obtain a solution. Additionally, transport equations with the corresponding coefficients and parameters for the discretization methods need to be defined [18]. All these operations can be selected in forms of Models. The following Table 6.5(p.35) shows the Physics Models which were used. In addition the last column gives an overview of alternative models.

For this thesis the Eulerian multiphase model was used. In the Eulerian description particles of the phases are captured at a fixed point. Alternatively, STAR-CCM+ provides the Lagrangian multiphase model which describes the movement of particles along a trajectory and should be used for modelling dispersed flows. It has to be taken into account that a discretization error occurs, because the model assumes for all phases the same velocity, pressure and temperature field in each control volume [18]. In addition, a modelling error could occur, if the water surface moves intensively, so that air enters the water body and water droplets goes into the air. In this case a very fine grid has to be chosen to reduce the discretization error. This complex surface movement occurs in shock waves.

The Physics Models are part of the Continua and after activating them, the Continua contains the initial conditions. The appropriate conditions and values are of great importance for the set up of the simulation and have a strong influence on the results. The initial conditions can be integrated in several objects and are mostly defined as constant values, but also Field Function are common. For the simulation the Field Function, Initial Fluid Fraction Equ. 6.2, was selected for the initial condition of Volume Fraction of water in the Continua object. The Pressure was defined by a Field Function named Pressure term:

$$(\text{\$Position}[2] <= 2.8185) ? (1000 \cdot 9.81 \cdot 2.8185 - 1000 \cdot 9.81 \cdot \text{\$Position}[2]) : 0 \quad (6.3)$$

This Field Function ensures a hydrostatic pressure distribution for the initial condition. For the velocity node a vector value was defined including the calculated inflow velocity in the y-direction.

Type of Model	Selected Model	Description	Alternative
Space	3D	3D meshes regarded, avoid one-cell thick 3D meshes	Axisymmetric, 2D
Motion	Stationary	no mesh movement required	DFBI, Morpher, Moving Reference Frame, Rigid Body Motion
Time	Implicit Unsteady	Activates Segregated Flow Model and Implicit Unsteady solver (check time-step size and the update at each physical time to obtain convergence); time-dependent	Explicit Unsteady, Harmonic Balance, Steady
Material	Multiphase Mixture	enables the Eulerian Multiphase model: specifies 2 phases (air and water)	Gas, Liquid, Solid, Multi-Component Gas, Multi-Component Liquid
Multiphase Model	Volume of Fluid	2 immiscible phases leads to free surface effects	Multiphase Segregated Flow
Viscous Regime	Turbulent	flow is irregular, vortical with wide range of scales	Inviscid, Laminar
Reynolds-Averaged Turbulence	K- ϵ Turbulence	quite robust and accurate	K- ω -, Reynolds Stress-, Spalart-Allmaras Turbulence
Optional Physics Models	Gravity	gravity effects, because of free surface flow	
	Segregated Fluid Isothermal	constant temperature	1D Coupling, Passive Scalar, Thin Film, Radiation, Turbulence Suppression, Cell Quality Remediation, Surface Tension, VOF Waves, Broadband Noise Sources, Lagrangian Multiphase

Table 6.5.: Physics Models. Overview of the selected model and alternative models

6.2.3. Solving

In the following, an overview of the different solvers and Stopping criteria is given. Furthermore, the terms under-relaxation factor and the temporal discretization scheme will be introduced. Selecting the models which are accurate for the simulation is of main importance. The models have an influence on the solution and hence on the Solvers. Their main task is to check the iteration and solution. STAR-CCM+ disposes over the Explicit and Implicit Unsteady Solver and appears by selecting the appropriate Unsteady model. With this Solver the Solver Frozen can be activated which means, that the Solver is not updating the solution during the iteration procedure. If it is deactivated the solution will be updated. The activated Solver Frozen is more a debug option and should not be used in the simulation process. Also the Implicit Unsteady Solver consists of this property. In case an Implicit Unsteady Solver is chosen the time-step size and the completion at each physical time will be controlled. With this Solver node it is possible to choose

between a first-order or second-order upwind convective scheme. More Solvers occur when defining a movement of the mesh or reference frame [18]. These solvers and also others are not part of the thesis and no further explanation will be done. In this thesis the flow regime is unsteady and hence the Implicit Unsteady Solver was chosen. The solver introduces the following parameters and temporal discretization scheme:

Solver	
Time-Step	0.5 s
Under-Relaxation Factor	0.8
Fluid Under-Relaxation Factor	0.8
Temporal Discretization	1st-order

Table 6.6.: Solver parameters

The mentioned default relaxation factors are set to 0.9, but to ensure convergence the mentioned factors were decreased to 0.8.

6.2.4. Post-Processing

The post-processing tool is supposed to filter out the relevant values of the variables which were calculated at each mesh point. STAR-CCM+ is equipped with different analyzing tools to export data to an ASCII file where they can be edited with e.g. Microsoft Excel. Besides this tool, the values can also be visualized with the different plotting tools the program possesses of.

Exporting plots of the scalar or vector scene can easily be achieved by producing a Hardcopy. For the visualization of the water surface an Iso-Surface was created. The Iso-Surface represents the volume fraction of water for cells which are half filled with water and half with air.

The velocity and the water level are the most relevant variables for this thesis. STAR-CCM+ enables to export the examined variables in form of a .csv file. The values are defined in the Tabular node of the simulation window. Because the velocities in the reservoir and the water level for the shock waves were measured along cross-sections, it is useful to export only the values of these areas.

In STAR-CCM+ the cross-sections can be defined as plane sections. A plane section is generated by defining the x-, y- and z- coordinates of the origin. For the orientation of the plane section a normal vector has to be defined. For this thesis, the coordinates for the origin are the coordinates of the first point of each cross-section. For the normal coordinates the angle of each cross-section had to be specified. The coordinates of the first point as well as the angle were determined by AutoCAD. The values for the normal direction were calculated by using the unit vector along the cross-section. The following picture helps to understand how the normal direction was calculated:

Equation 6.4 to 6.6 can be derived from the unit vector:

$$x_n = y = 1 \cdot \sin \varphi \quad (6.4)$$

$$y_n = x = -1 \cdot \cos \varphi \quad (6.5)$$

$$y_n = 0 \quad (6.6)$$

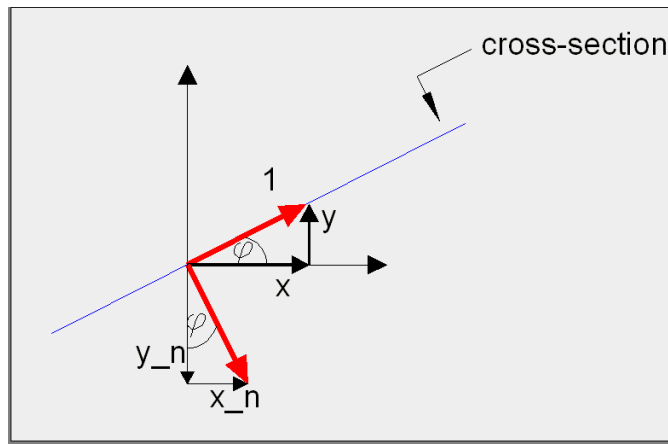


Figure 6.4.: Derivation of the normal direction of the plane sections

The velocity vectors of each cross-section can be visualized on the plane sections. In the physical model, the water level was only measured for the shock waves. But also for the evaluation of the velocity measurements the water level had to be known. Therefore, the water level for each measuring point was extracted from the simulation. This is quickly done by copying the plane sections and instead of applying the whole geometry the Iso-Surface was applied. This treatment gives the water line and the values can be exported in form of a Tabular file. Plane sections were also created for determining the water level between dam and bridge pier where the shock waves occur.

6.3. Mesh Generation

The choice of the right mesh is very important and a good understanding of meshes should exist. The main purpose of using meshes is to divide the computational geometry into cells or control volumes. Depending on the discretization method the values of the variables are computed in the cell center or on the boundary. The shape of the cell can have different forms corresponding on the used CFD software. Structured mesh codes support triangular (2D) and hexahedral (3D) cell shapes whereas unstructured mesh codes use triangular forms in 2D and tetrahedral or polyhedral forms in 3D. The mesh should be generated that the adjacent cell faces are always connected to each other. A crucial part in mesh generation are the regions close to walls. These regions correspond to a high gradient in e.g. velocity and hence a finer mesh with adequate cell shapes are required [20].

The number of faces or cells depends on different factors like cell shape, mesh structure or cell size, only to mention some of the factors. There exists a wide range of different mesh types, but only the mesh categories supported by STAR-CCM+ will be explained further. Generating grids in STAR-CCM+ is a simple procedure due to the predefined mesh tools. Paragraph 6.2.2 introduces the different categories of meshes of STAR-CCM+.

6.3.1. The Choice of Mesh

STAR-CCM+ uses both a structured and unstructured mesh solver. Unlike a structured mesh, where each grid point has a corresponding integer (i, j, k), the cells are not lying along parallel

lines and the number of cells are varying along the three directions. The mesh can not be described by integers like for a structured mesh. The unstructured mesh seems to be chaotic with cells distributed randomly over the geometry. With unstructured meshes it is possible to model complex geometries. Figure 6.5 shows the difference between a structured and unstructured mesh [20].

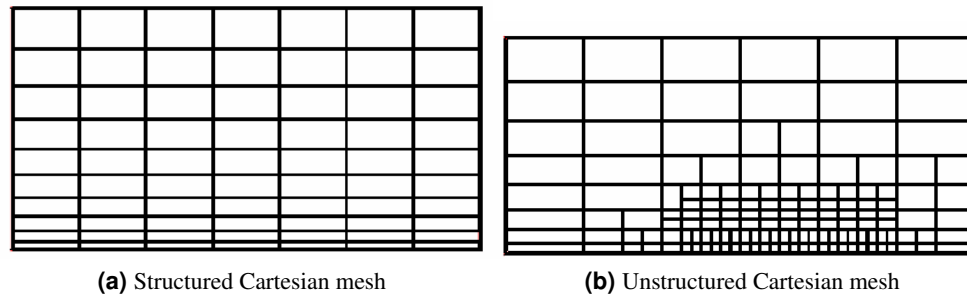


Figure 6.5.: Overview of a structured and unstructured mesh

STAR-CCM+ is based on orthogonal as well as on non-orthogonal mesh structures. In the latter case, the angle between the vertical and horizontal grid lines differs from 90° and for orthogonal grid the mesh lines have to cross each other perpendicular. For the determination of the variables at a specific point of interest on a non-orthogonal grid a curvilinear coordinate system, like described below for a body-fitted mesh, has to be applied [3]. Consequently, non-orthogonal meshes are more flexible, but also implicate higher computational cost.

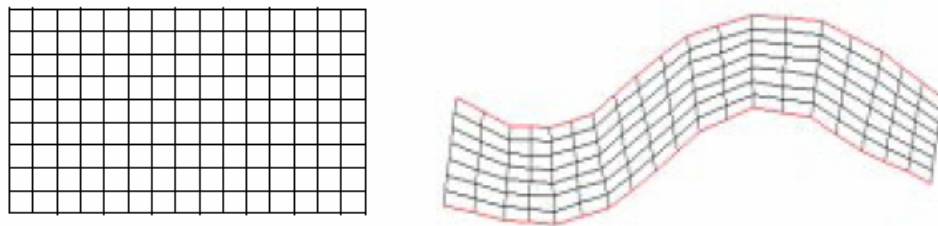


Figure 6.6.: Difference between orthogonal (left) and non-orthogonal mesh (right), [3]

When flows are regarded which are passing objects, in this case gates and piers, or are following a curved river bed, it is extremely useful to use a body-fitted mesh. The coordinate system is aligned to the grid lines of a structured grid. The principle of a body-fitted mesh is to modify the Cartesian coordinates in such a way that they fit smoothly around the boundaries. The body-fitted mesh, also known as curvilinear mesh, is generated automatically and has the advantage of converging faster. Furthermore the mesh has a higher robustness for complex geometries, is achieving a good representation of the geometry and is able to fill the gap through mesh refinement. The mesh refinement allows a higher resolution at specific points of interest [20]. The other mesh technique which was used to represent the objects in the simulation as best as possible was the nested mesh. Easily described a nested grid is a fine mesh inside a coarse mesh. The coarse mesh can be large, but the fine mesh is limited on a certain region inside the larger mesh and has to be specified for the desired flow condition. Nested grids are mostly used to represent areas with high gradients [3]. Furthermore, for the simulation was only a single-block mesh used. With the nested mesh technique a better representation of the geometry and hence of the flow was achieved. For this thesis, a nested mesh containing of two meshes was built around the gates and piers. The construction of the nested mesh is described in 6.2.2

7. RESULTS

This chapter contribute to find out how well the simulation is able to replicate the flow phenomena of the physical model. For this thesis three simulations were run. For comparing the velocity measurements two simulations based on a polyhedral mesh and trimmed mesh were performed. For the shock wave simulation a trimmed mesh was chosen. These two mesh types were chosen to compare orthogonal with non-orthogonal mesh. Which mesh is representing a better correlation by comparing the measured values with the calculated values will be discussed in paragraph 7.1.3

After completing the simulations the values for both the velocities and water level could be exported in form of tabular data. The following paragraph includes the results of the measured velocities compared with the calculated velocities for both mesh types. Paragraph 7.2 introduces the evaluation of the calculated water level and the comparison to the measured values. The roughness height for the bottom boundary is set to 2 mm in all simulations, which represents a good-quality concrete.

7.1. Velocity Distribution

For both simulations a nested mesh for the dam as well as for the bridge pier was defined. The nested mesh has a block shape and the dimensions refer to the dam or bridge size. The size of the cells are about 10% finer than the base size which was defined to 0.1 m.

For each measuring point the water level was determined by STAR-CCM+ and could be exported in an ASCII-format. For each cross-section two data sheets had to be evaluated. The water surface corresponding to the spatial coordinates, x and y, was given in one spreadsheet. With this spreadsheet the water level for each measuring point could be determined. Knowing the water level the velocity in x-, y and z-direction could be determined by the second spreadsheet. It consists of the three velocities, the spatial coordinates, x and y, as well as the water level. For each water level the correct x- and y- coordinate of the measuring points had to be found out and for these coordinates the velocity could be determined.

The u-velocity is the velocity in flow direction. The v-velocity is defined as the velocity in lateral direction and the z-velocity represents the velocity in the vertical direction.

Figure 7.1 shows the cross-sections with the velocity vectors and the volume fraction for the trimmed mesh. In Figure 7.1(a) the secondary flow area on the left side in flow direction can be observed. In Fig. 7.1(c) it can be seen that the velocity vectors in the middle of the cross-section 51 are directed against the flow direction. The cross-section 51 is positioned in front of the bridge pier which influences the flow. Furthermore cross-section 51 shows higher velocity values than the other cross-sections. This is because cross-section 51 is in a contraction which accelerate the flow.

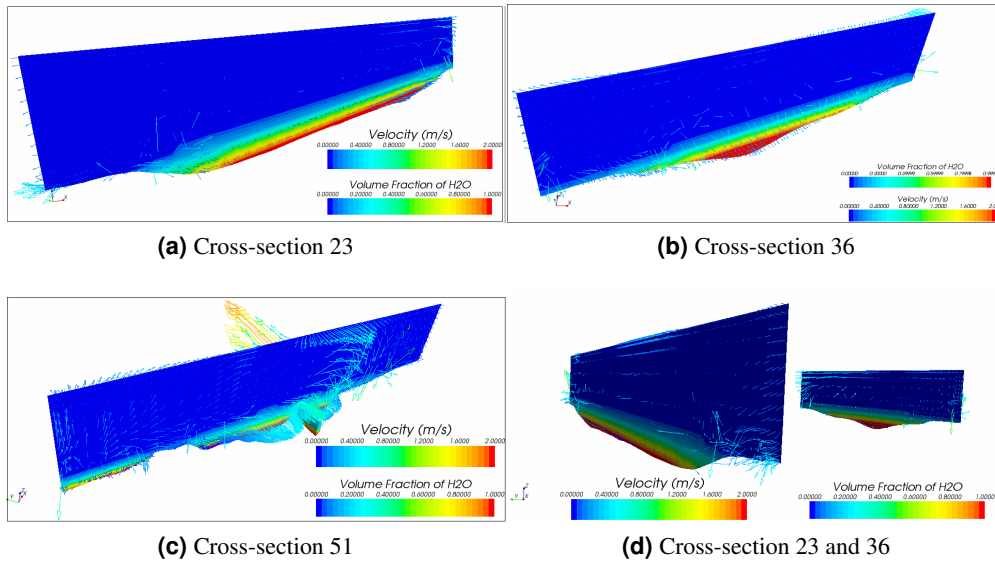


Figure 7.1.: Velocity distribution for the trimmed mesh, downstream view (a)-(c), upstream view (d)

7.1.1. Polyhedral Mesh

Figure 7.2 contains the measured and calculated velocities for each direction of cross-section 23. Each Figure contains of four graphs - the transformed velocity (Equ. 3.2) measured with the Vectrino Velocimeter $\langle \mathbf{u} \rangle$, the calculated velocity \mathbf{u}_{calc} , the water surface z_{surface} and the river bed elevation z_{bed} . The water surface are the values from the simulation. The measurements were taken place from the right to the left side of the physical model.

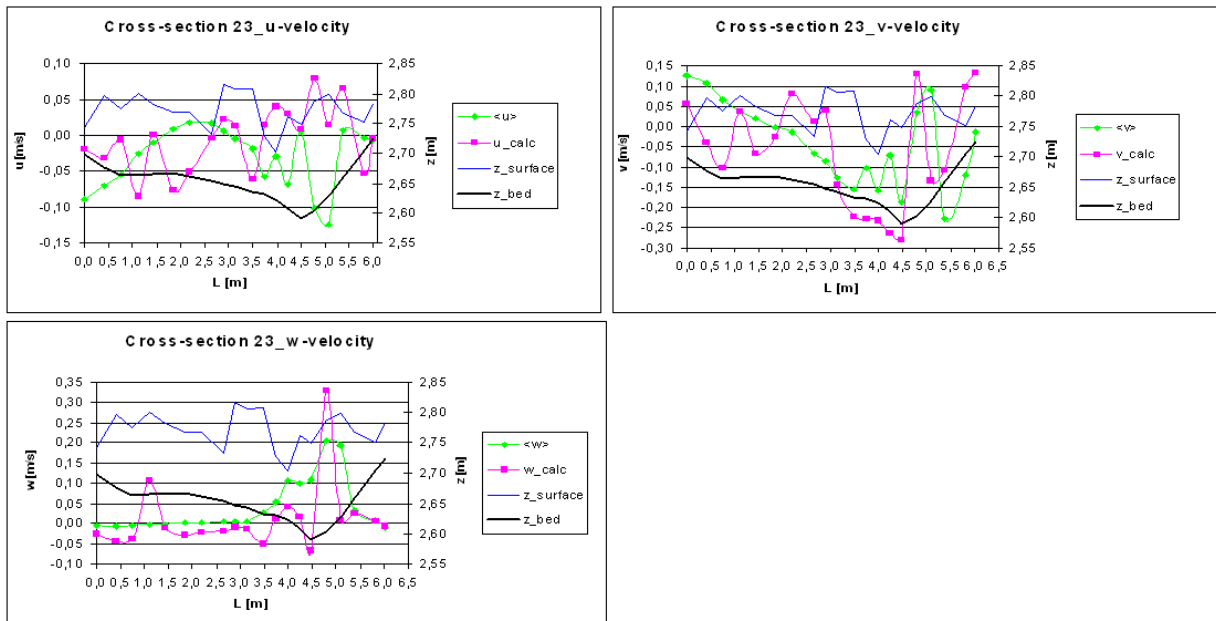


Figure 7.2.: Measured and calculated velocities with water surface and river bed of cross-section 23

For this cross-section the measured velocities differ extremely from the calculated velocities. The calculated velocities are fluctuating strongly whereas the measured velocities, at least on the right

side, follow an uniform distribution for all three plots.

The measured u-velocity is in the range of $[-0.124, 0.019]$. The calculated velocity has a higher maximum value and a smaller minimum velocity $[-0.085, 0.080]$. The maximum averaged velocity is however found in the vertical direction for both velocities. For this cross-section, it is difficult to make a clear statement about which velocity has higher values or lower values.

The graphs of the vertical velocities shows for both velocities strong fluctuations on the left side. On the right side however the measured velocity is much more uniform and the calculated values are fluctuating strongly over the whole cross-section. For understanding the source of this velocity distribution the topography (black graph) of the river bed should be regarded. The topography of the cross-section 23 is varying. On the left side is a secondary flow area which is confirmed by the vertical velocity distribution. The values for both velocities are more unstable and mostly greater than at the beginning of the cross-section. On the right side is the flow phenomena almost undisturbed and no dominant vortices occur. The vertical velocities are, except of one peak value in the calculated velocity, more flat and uniform. This distribution is similar to the y-direction.

Unfortunately, the measured values do not match the calculated velocities. The flow examined on cross-section 23 might have been influenced by the inflow. The measurements were conducted with a highly non-uniform inflow. For considering the turbulent inflow in the simulation, the turbulent kinetic energy and dissipation rate can be defined. This however was not taken into account, because the turbulent length scales could not be specified.

Figure 7.3 shows the velocity distribution for the measured and calculated velocities at cross-section 36. This cross-section is much more narrow than cross-section 23. Furthermore, it has a higher water depth and is further away from the turbulent inflow.

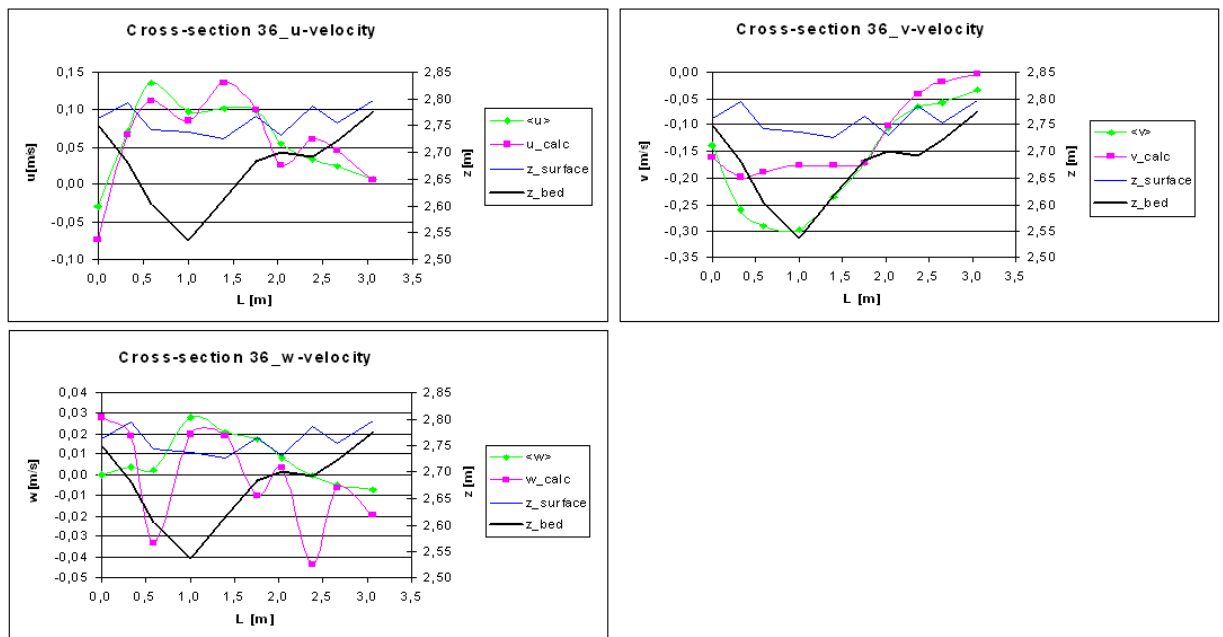


Figure 7.3.: Measured and calculated velocities with water surface and river bed of cross-section 36

For this cross-section the measured velocities match much better with the calculated values compared to cross-section 23. The shapes of the two velocity graphs for the x- and y-direction are quite similar. Both velocity distributions show less fluctuations, except for the calculated vertical velocity. Both u-velocities are higher compared to the u-velocities in the previous

cross-section. The measured u-velocity is in the range of $[-0.03, 0.136]$ and the calculated values are in the range of $[-0.07, 0.136]$.

The topography of the cross-section is characterized by a deep cut on the right side (black graph). Measurements were conducted on a slope for point 2, 3 and 5. The boundary of the cut might influence the measurements. The Vectrino Velocimeter could not be positioned straightly which implies a different orientation of the transmitted beam. Consequently, the velocities have a different angle and the sampling volume could not be specified at the horizontal distance of 5 cm in front of the transmitter. The Vectrino Velocimeter might have detected some incorrect velocity measurements.

For the vertical velocity distribution it is noticeable that the calculated velocity is higher than the measured values. Both velocities have negative values which indicate the existing of reverse flow. The calculated vertical velocity is quite high and shows a fluctuating distribution. On the river bed are acting shear stresses which implicate a high velocity gradient. This gradient can lead to a replacement of water parcel which are close to the boundary and have a small velocity compared to the water parcel in the inside of the flow. This indicates a turbulent flow and could explain the high vertical velocities.

Figure 7.7 depicts the velocity distribution of cross-section 51. The cross-section is positioned close to the upstream side of the bridge pier. The graph of the bed elevation might not be accurate, because this cross-section is not part of the provided cross-sections.

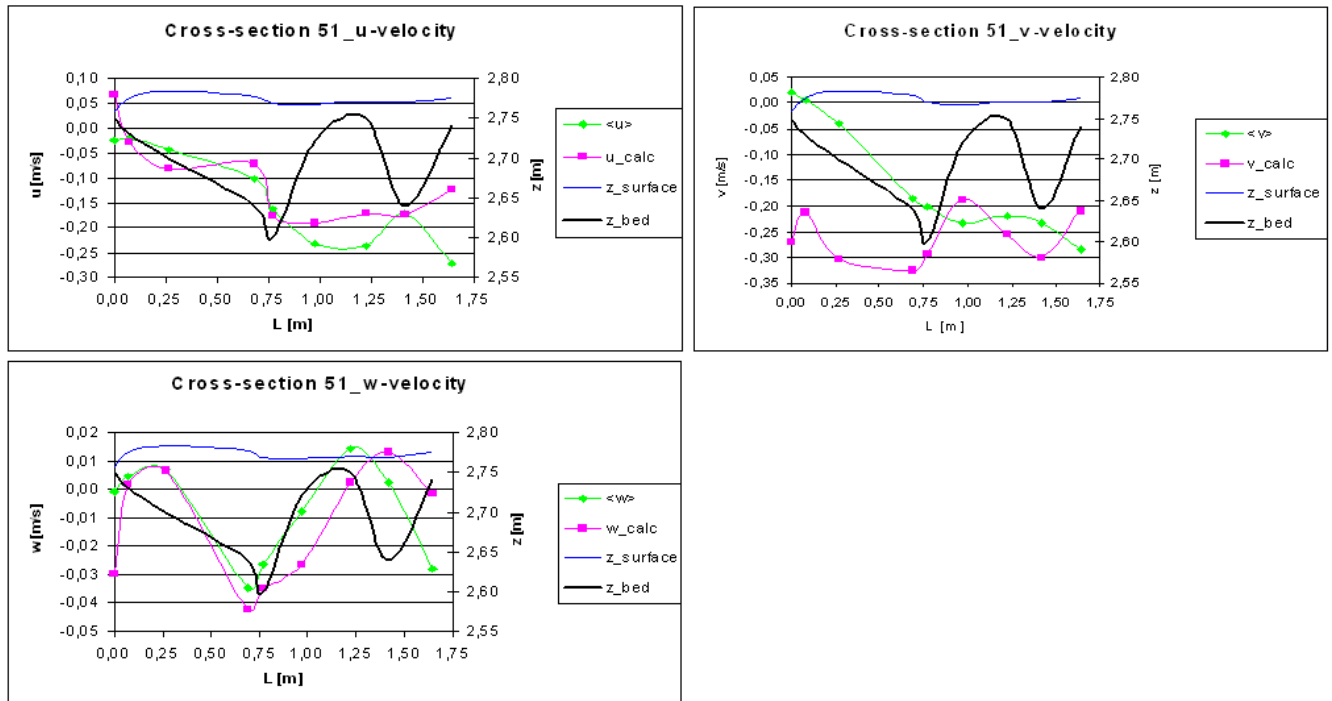


Figure 7.4.: Measured and calculated velocities with water surface and river bed of cross-section 51

The velocity graphs fits quite well for the u- and w-velocity. The velocity distribution of the measured velocity for the v-velocity shows great differences to the calculated graph. The velocities have mostly negative values. The reason might be that the water level of this cross-section is influenced by the bridge pier and river bed. The river bed is characterized by two cuts. In these regions the flow can form recirculation areas which could influence the upstream flow and causes a reverse flow. Additionally the flow is disturbed by the bridge pier and river bed which might cause the water to flow against flow direction.

7.1.2. Trimmed Mesh

Figure 7.5 depicts the velocity distribution for the measured and calculated velocity in x-, y- and z-direction. The results are based on a trimmed mesh.

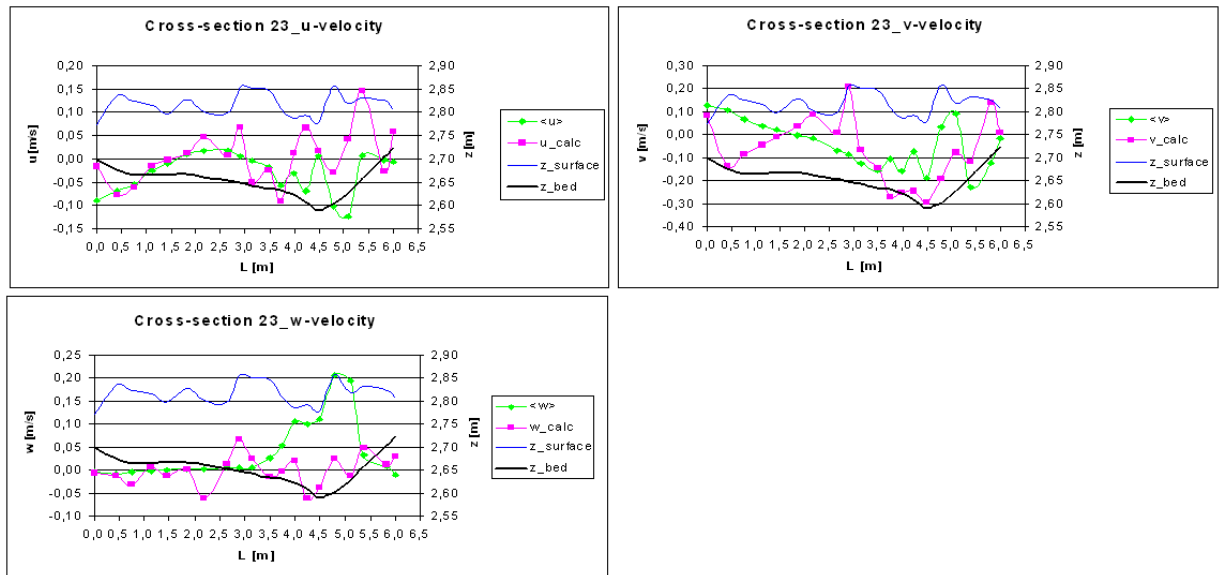


Figure 7.5.: Measured and calculated velocities with water surface and river bed of cross-section 36

The measured velocities show in all three directions an uniform velocity distribution on the right side. The velocities start fluctuating in the middle of the cross-section and maintain this distribution to the end of the cross-section. The reason for the fluctuations is, like mentioned above, the existing of a secondary flow area.

The measured and calculated u-velocity match quite well on the right side and deviate from each other in the secondary flow area. In this area the calculated u-velocity shows compared to the measured u-velocity higher values.

The v-velocity graphs present a poor correlation. The assumption that the calculated velocity at the beginning of the cross-section match better to the measured velocity was not satisfied. The water depth of the area is low and the flow is free of vortices. Both vertical velocities confirm this assumption by showing a smooth velocity distribution. The two graphs are not matching in the secondary flow area. The measured values are much higher.

The calculated lateral and vertical velocities do not represent the flow in the secondary flow area correctly. The graphs shows fluctuations, but these are too small.

Figure 7.6 shows the three plots of the velocity distribution in cross-section 36 using a trimmed mesh. The topography of the river bed is characterized by a deep cut. The calculated velocity for the three graphs deviates in the cut more from the measured values as on the right or left side. This might have the reason that the Vectrino Velocimeter could not positioned straightly above the measuring point lying in this cut.

For the velocity in y-direction the two graphs fit quite well and only two values deviates strongly from each other. The calculated vertical velocity fluctuates more compared to the measured values. The calculated u- and w-velocity of point 5 in measuring direction protrude extremely with a peak value of $u = 0.195 \text{ m/s}$ and $w = 0.08 \text{ m/s}$. The position of the point is on the slope of the cut. It might be that the Vectrino Velocimeter was not detecting the velocities correctly, because the minimum distance of 5 cm was not adhered.

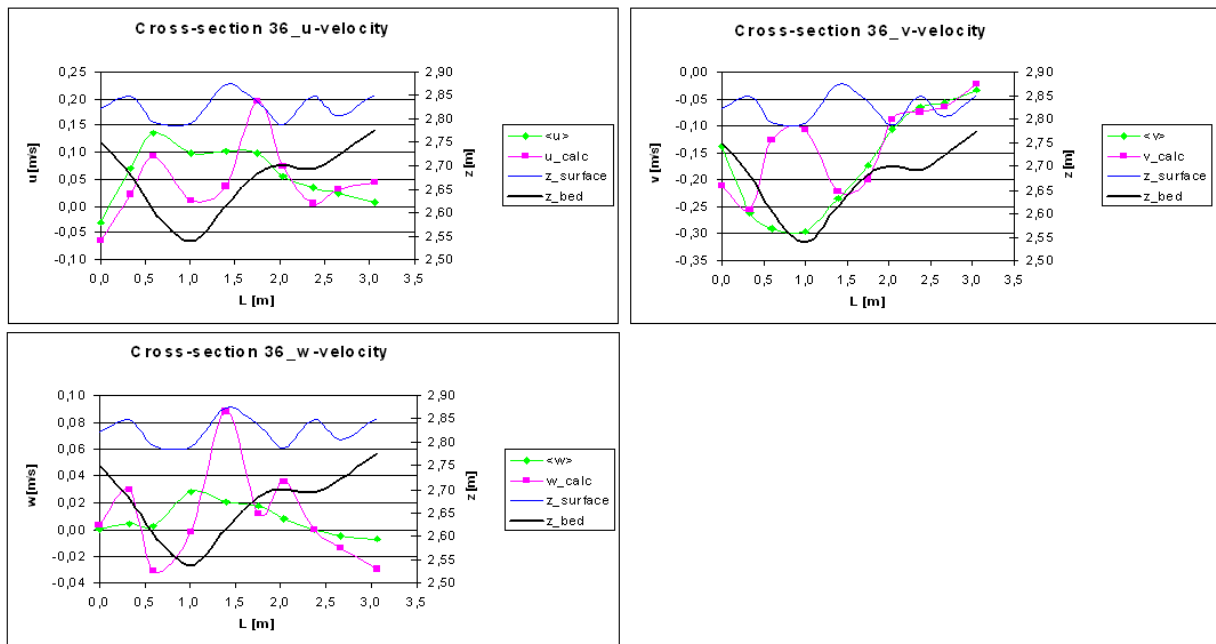


Figure 7.6.: Measured and calculated velocities with water surface and river bed of cross-section 36

Figure 7.7 represents the velocity distribution of cross-section 51. The two velocity graphs show

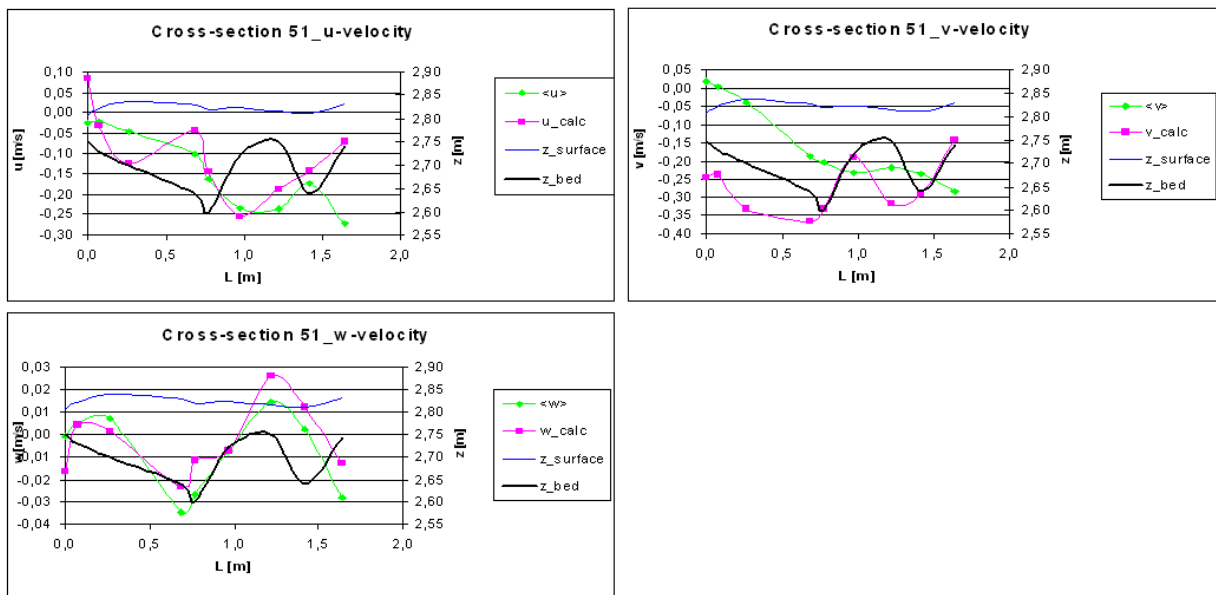


Figure 7.7.: Measured and calculated velocities with water surface and river bed of cross-section 51

a good correlation in flow direction as well as in the vertical. The calculated velocity in y-direction is mostly much smaller compared to the measured values. Furthermore the calculated velocities show a more unstable distribution. The maximum values of the calculated velocity is achieved at the last point, whereas the measured value has the maximum value at the first point and the values are decreasing along the cross-section. The topography of the cross-section is also very bumpy with two cuts in the geometry. Measuring points were also marked within these cuts. It could also happen that the Vectrino Velocimeter was positioned that the minimum distance to

the wall was not satisfied. The velocities in flow direction are quite small (smaller than zero with one exception). The side boundaries are almost straight and the flow velocity reduces on the boundary and indicate a high gradient. This can cause eddies which lead to a non-uniform flow. Both graphs of the vertical velocities are characterized by high values and a fluctuating distribution.

7.1.3. Discussion

STAR-CCM+ computes the water level and the velocities in the cell center according to the Finite-Volume method. Using a coarse grid means that less data is provided. The trimmed mesh consists of 469,042 cells and is much coarser than the polyhedral mesh which consists of almost 2 million cells. That means that on a coarse mesh less calculation were performed.

For both simulations an iterative error occurred. The individual graphs of the residual plot are oscillating around the correct values. Reducing the mesh size and time-step increases the computational time. The time-step is correlated to the inner iteration and decreasing the time-step means that more inner iterations have been calculated. Several simulations were performed to lower the values and to reduce the oscillations. For keeping the computational time as short as possible the time-step was set to 0.05 and the iteration to 20 which is quite high. Furthermore the base size of the mesh was limited. For small mesh sizes (low range of cm) a problem with the virtual disk space of the computer occurred.

The residual plot for the two mesh types are shown in Figure 7.8:

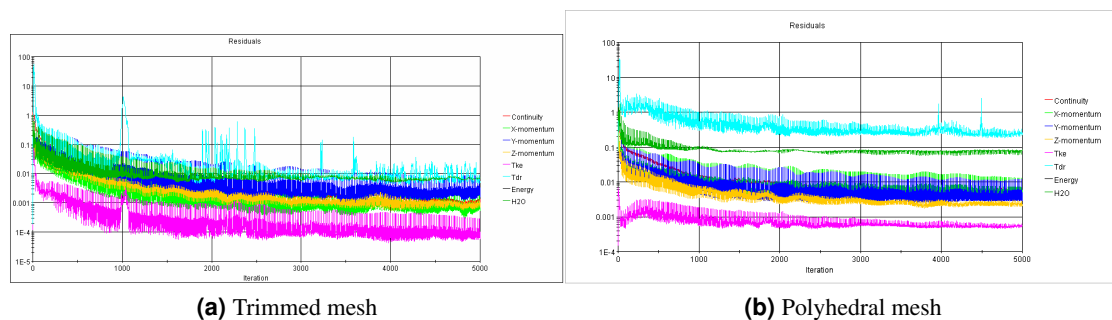


Figure 7.8.: Residual plots

The residual plot of the trimmed mesh shows better convergence even with less cells than the polyhedral mesh. For both mesh types a problem occurred finding the spatial coordinates (x and y) for the corresponding water level. Hence, for the correct water level the coordinates were found by an averaging process. This was however difficult and time-consuming. Comparing the velocity graph of the polyhedral mesh with the trimmed mesh results in not many differences. For cross-section 23 the calculated velocity distribution shows more fluctuations even in area of small and uniform water flow (right side). The velocity graphs in flow and vertical direction match better for the trimmed mesh. Both meshes are not showing a satisfying velocity distribution in y-direction. The velocity range is almost the same for both mesh types with few exceptions. For cross-section 36 the trimmed mesh shows slightly better results than with the polyhedral mesh. The velocity range of all velocities is for both mesh types almost the same. Also cross-section 51 does not show any great difference between the individual graphs. The graphs have the same shape for all velocity plots. The velocity range is also not showing a big difference. For the z-velocity of the polyhedral mesh the measured velocity is higher than the calculated and vice versa for the trimmed mesh.

7.2. Shock waves

The simulation was performed on a trimmed mesh based on orthogonal mesh lines. The volume mesh consists of about 3,2 million cells and includes a nested mesh between dam and bridge pier. A second nested mesh was applied after the simulation time of 140 s. The mesh was positioned upstream of the first nested mesh. A restart was performed to run the simulation for 10 s physical time which gives a total computing time of 150 s. The Base Size of the coarse mesh was chosen to 0.08 m. The nested meshes have a relative size of 20 % and 30 % of the coarse mesh. Figure 7.9 shows the shock wave of the simulation and the measurements designed with Tecplot.

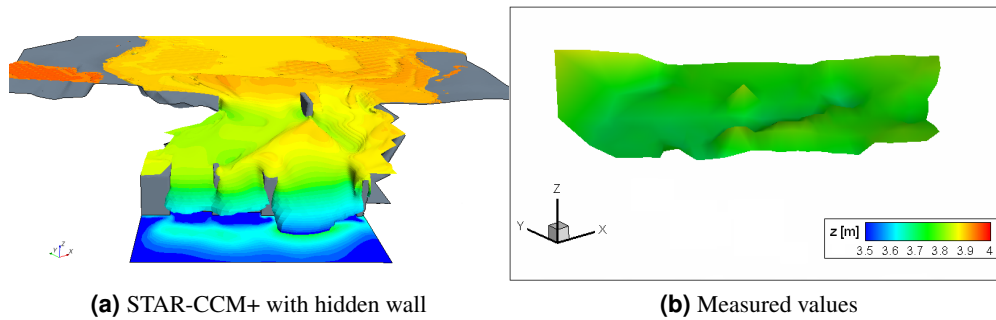


Figure 7.9.: Shock wave

Comparing the simulation with the measurement in Figure 7.9, gives a first overview of how the shock waves can be replicated by STAR-CCM+. On the right side of both figures the water level is almost in the same range. The water level of the simulation shows an extreme influence of the bridge pier. Close to the pier starts the shock wave which is increasing its size until the flow is passing the dam. The water pile up on the left side is not compatible to the measurements which shows smaller values. The measurements look more flat and the shock wave was not replicated in such a way. For getting a better overview of the calculated and measured shock wave the water level of each cross-section has to be examined.

For the evaluation of the calculated water level, plane sections were constructed to replicate the cross-sections of the physical model. Each plane section is defined by an origin and normal vector. For the origin values the coordinates of the first measuring point was chosen. The coordinates could be specified with AutoCAD. The normal values were defined by the unit vector (see Equ. 6.6). For obtaining the water levels the water surface line had to be defined. The plane sections were copied and only the Isosurface, which represents the water surface, had to be chosen. STAR-CCM+ is able to export the values as an ASCII file. The table consists of the spatial coordinates (x,y) and of two values for the water level which were almost equal. With this table the water level for each measuring point could be specified.

Figure 7.10 shows the measured and calculated water level distributions. The measurements were taken place from the right to the left side.

Both graphs of each plot show a good representation of the shock waves. The calculated water level is in general 8 cm higher than the measurements. The reason for these differences might be the simplified outflow boundary condition. For Fig. 7.10 (a) to Fig. 7.10 (d) the calculated water level match the measurement graph quite well. At the end of each cross-sections (left side in the physical model) the difference between both graphs is greater. The reason might be the channel which is positioned on the left side of the dam. The water passing this channel enters an outlet. The valve of this outlet were not completely closed and a discharge of $Q = 8 \text{ l/s}$ was recorded.

The partly open outlet was on purpose to avoid overspilling water from the channel boundary which could influence the flow over the dam construction (refer to Fig. 7.9 (a)). The flow in STAR-CCM+ was simplified and the small discharge was subtracted from the incoming flow which originally was set to $Q = 100 \text{ l/s}$. The flow phenomena directly upstream of the dam could also be pretty well replicated by the simulation.

7.2.1. Discussion

STAR-CCM+ is able to replicate complex flow phenomena like shock waves. Even if the calculated values do not match the measurements completely the results are quite satisfying. For further work it is recommended to ensure the exact flow condition for the simulation and physical model. Moreover a very important aspect is to measure the water level on many points. The area in which the measurements were conducted was filled with a relatively dense net of measuring points. The distance between the cross-sections is around 16 cm and should be reduced for further studies. The mesh of the simulation was fine enough to find the correct water level to the corresponding spatial coordinates. Unlike for the water velocity evaluations the values were quite easy to find and no averaging was needed. A finer mesh means more cells and hence more calculation were performed during the simulation. Furthermore the cells lie closer together which means that the coordinates of the points provided by the simulation match more accurate to the measurements points. Fig. A.3 shows the residual plot of the shock wave simulation.

The simulation was not able to satisfy convergence and the residuals were oscillating around the averaged value of 0.001. Convergence should be improved to provide better results of the simulation. Another source of error might be that the provided cross-sections do not cover the river geometry correctly. The coordinates were measured in winter and a thick ice layer disabled measurements especially on the sides of the river. Measurements conducted by the staff of the Vassdragslaboratoriet show that the discharge did not fit to the water level. This was fixed after the measurements for the thesis were conducted.

Even with this inadequacies STAR-CCM+ is able to provide a satisfying replication of the shock waves.

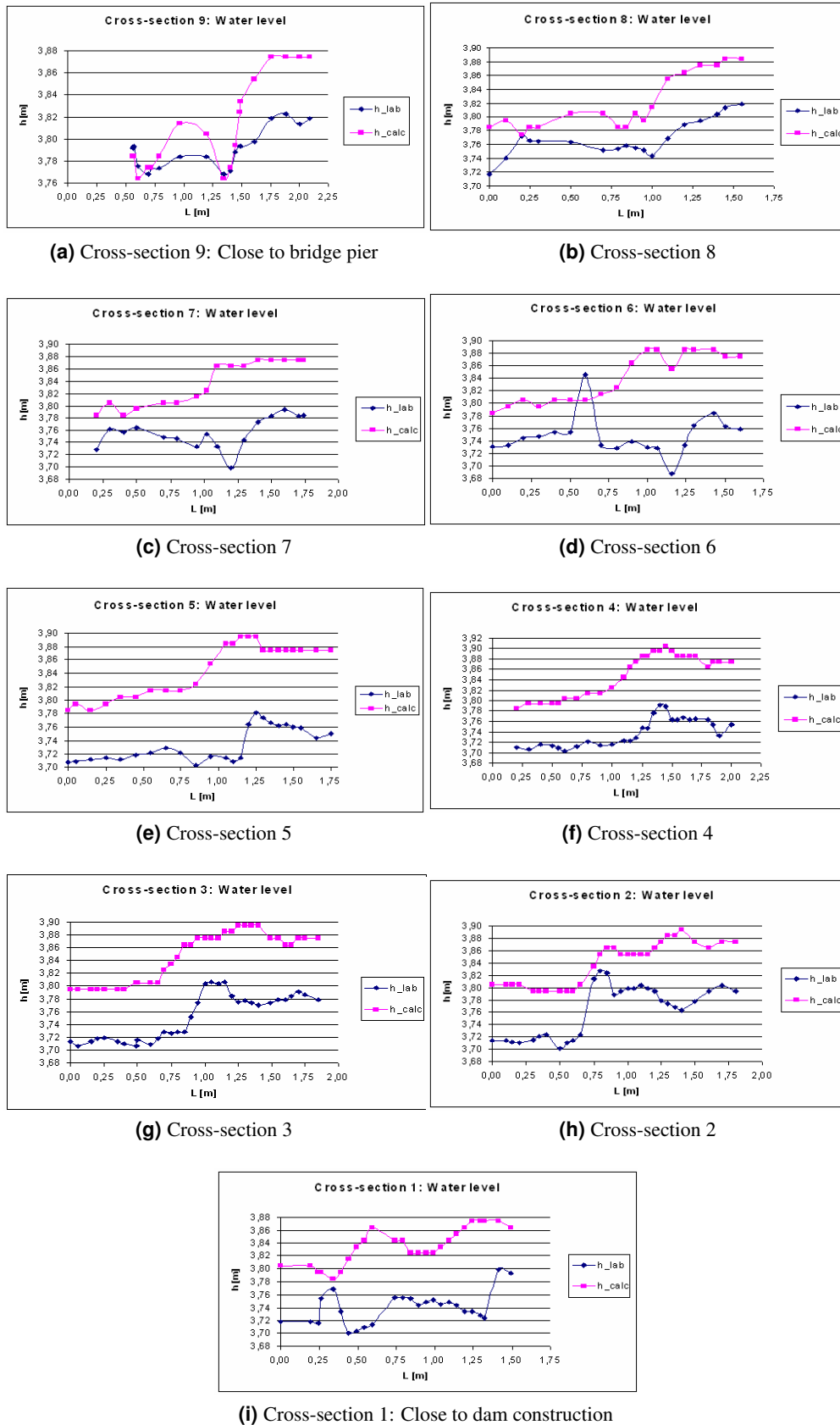


Figure 7.10.: Water level graphs of the measured (blue) and calculated values(rosa)

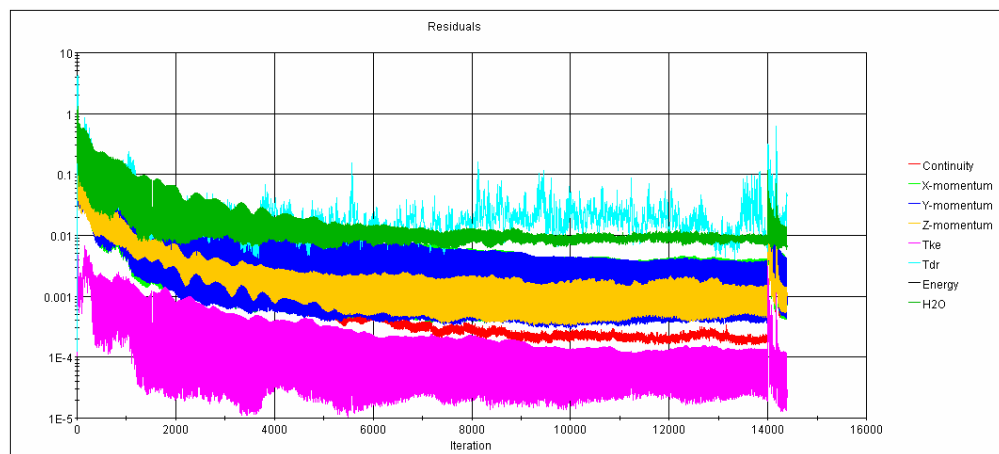


Figure 7.11.: Residual plot of the shock wave simulation

8. CONCLUSION

The main task of this thesis was to find out how well flow phenomenas occurring in the physical model can be reproduced with the CFD program STAR-CCM+. The possibility of simulating complex flow phenomena, like shock waves, is a big incentive among researchers. Physical model testing is mostly very expensive, time-consuming and demanding lots of space, but the main advantage is the concreteness of investigating flows. Furthermore the results are available after a short time. CFD programs are very complex and are based on many algorithms. Although the purchase of commercial CFD programs are immense, but in respect of investigating different flow phenomena make them affordable. Adjusting the boundary conditions can be done in a short time. One of the disadvantages is that the simulations need a long time to get the desired variables.

The water velocity in the reservoir and the water level between dam and bridge pier were measured. These measurements were used to test STAR-CCM+. For the water level measurements a higher discharge was used. The focus was to test STAR-CCM+ in respect of the shock waves. Shock waves have not been investigated with a commercial program quite often. For the water velocity measurements three different cross-sections were chosen under the aspect of determining secondary flow areas or the influence of a bridge pier.

The simulations were performed under the aspect to replicate the physical model with all the special flow phenomenas as accurate as possible. The geometry was designed in AutoCAD. The physical model consists of intakes which were not taken into account and only the provided cross-sections were used to construct the river bed and vertical side walls. The dam construction with the three gates (closed) and the rounded dam pier were designed together with the bridge pier, upstream of the dam, separately with AutoCAD. The dimensions were measured in the physical model to ensure the best replication as possible.

The tested velocities were measured with a Vectrino Velocimeter. The measuring instrument with a side-looking probe was well suited to measure the water velocity in open channel hydraulics. Unfortunately the results of the calculated water velocity were not very satisfying. The non-uniform inflow of the physical model might be the reason for it. For the simulation was the inflow simplify to a uniform velocity distribution. This has impact on the calculated velocities especially on cross-section 23 which is close to the inflow. For the two other cross-sections the measured water velocity fit quite well to the calculated values. Although the secondary flow areas could be replicated in the simulations.

For the shock wave measurements a higher discharge was adjusted to emphasize the wave features. Furthermore the gates were open which could be quickly designed by AutoCAD by changing the geometry which was already designed for the closed gate position. The simulation set up was the same as for the closed gates, except of the different discharge resulting in adjusting the inflow water velocity and water depth. The calculated water level is for all cross-sections

higher than the measurements. Both graphs of the water surface show a similar shape. The deviations are based on the different boundary condition of physical model and simulation.

CFD programs like STAR-CCM+ are very complex and simulations can be run under the aspect of different parameters, e.g. using kinetic and dissipation scales to replicate the non-uniform inflow or time-step. The results could probably be better if the simplifications would have been avoided. Moreover the evaluation of the simulations were performed although the residuals were not satisfying convergence. Further studies of these flows are recommended to get more experience to replicate complex flows with STAR-CCM+.

9. RECOMMENDATIONS

9.1. Vectrino Velocimeter

The use of measuring instruments require a good understanding of the measuring procedure. Before the measurements are conducted it should be clear how the instruments works and what preparation are needed to ensure a trouble-free measuring process. When conducting measurements in a big reservoir as for this thesis and using measurement systems with little knowledge about them, it is very useful to practice with the instrument in a small basin or bucket before the important measurements have been started. Air bubbles at the receivers affect the measurements and have to be avoided. Moreover too clean water can cause noise in the velocity measurements. Noisy data can also occur when the velocity range is set too high. This can be avoided by estimating the water velocity before starting the measurements. Moreover it always has to be ensured that enough particles are in the water.

9.2. STAR-CCM+

STAR-CCM+ provides a user-friendly graphical interface which is built up like a tree, ensuring an orderly structure of the simulation. Each object of the simulation tree is subdivided by several pop-up menus which navigates the user easily through the set up of the simulation. Before starting a simulation it should be well considered if STAR-CCM+ is appropriate for the studies. When STAR-CCM+ is chosen as the program which best fit for the investigated flow case the following tips should provide an overview of some essential steps.

- Geometry and Flow

It is very important to have a good understanding of what should be simulated. STAR-CCM+ is well suited for importing CAD drawings. For importing the geometry in STL-format it has to be checked if the coordinates have positive values. This is very important and geometries with negative coordinate values are shifted due to an unknown factor.

For complex flow phenomenas like the shock waves the input data and boundary conditions are essential. Underestimating the initial flow discharge or the time the water needs to flow to the outflow can have negative impacts on the calculated variables. The boundaries should also be specified accurately due to the physical model or prototype. STAR-CCM+ is based on slip and non-slip boundaries. Moreover the program includes the use of Field Functions to apply non-standard functions instead of a constant value. For open channel flow STAR-CCM+ consists of the VOF method to calculate the free water surface. Flows which consists of different phases, like the open channel flow, the Eulerian multiphase flow can be activated.

- Mesh and Turbulence

STAR-CCM+ consists of different surface and volume mesh types. For the surface mesh it is recommended to use the Surface Remesher which is possible to repair the mesh if problems occur. The quality of the mesh can be controlled by starting the mesh diagnostics. For the volume mesh three different mesh types exist which are based on orthogonal and non-orthogonal meshes. For this thesis, the orthogonal mesh shows better results. STAR-CCM+ is suitable to compute laminar as well as turbulent flow. Different approaches for the turbulent flow are provided, like RANS and LES. For the RANS approach many turbulence models can be used. The most common model is the $k-\epsilon$ model, but it should be taken into account that this model is based on the assumption of isotropy. Furthermore, both steady and unsteady flows can be simulated. Besides the models the property of the fluid has to be determined.

- Results

The residual plot accompanies the simulation (like in Fig. ??). The residuals provide a control whether the solutions converge or not. If convergence is not satisfied, the simulation can be stopped and parameters can be changed to improve the stability and hence the convergence. The residuals should be as small as possible and all graphs should match and should not oscillate around a specific value. Mostly the values of the residuals decrease and become more smooth during the simulation. For satisfying convergence different parameters could be changed:

- Time-Step and Iterations: The time step corresponds to the number of inner iterations. A small time-step improves accuracy, but it also implicates more inner iterations. This leads to an increase of the computational time. Appropriate values for the time step and number of inner iterations should be found to satisfy the accuracy which is aspired.
- Relaxation Factor: The default values can be reduced to improve convergence. It is recommended to lower the values in small steps, because the converging process is longer for small values.
- Mesh type: The mesh type has an influence on the convergence and it should be checked which mesh type represents the flow as accurate as possible.

To continue the simulation it is always possible to use a restart.

- Post-Processing The post-processing is a very important tool for visualizing the solutions. STAR-CCM+ consists of different features which enable to plot the solutions in scalar (contours) or vector form or to plot variables in a diagram.

The STAR-CCM+ user guide consists of different tutorials which are appropriate to learn the software. The tutorials are based on different aspects of flow cases and they provide a first contact with the software.

Bibliography

- [1] B. Ruck. *Messverfahren in der Strömungsmechanik*.
[http://www.ifh.uni-karlsruhe.de/science/aerodyn/bilder_](http://www.ifh.uni-karlsruhe.de/science/aerodyn/bilder_originale/pub/M-pup/Thumbnails.html)
[originale/pub/M-pup/Thumbnails.html](http://www.ifh.uni-karlsruhe.de/science/aerodyn/bilder_originale/pub/M-pup/Thumbnails.html). Class notes: 2009.
- [2] ICOLD. *Spillways. ShockWaves and Air Entrainment, Bulletin 81*.
- [3] Prof. Nils Reidar B. Olsen. Numerical modelling and hydraulics.
- [4] Gravity dam design. [http://140.194.76.129/publications/](http://140.194.76.129/publications/eng-manuals/em1110-2-2703/toc.htm)
[eng-manuals/em1110-2-2703/toc.htm](http://140.194.76.129/publications/eng-manuals/em1110-2-2703/toc.htm), 1995.
- [5] Moffat A.I.B. Nalluri C. Novak, P. and R. Narayanan. *Hydraulic Structures*. Academic Division of Unwin Hyman Ltd, 1990.
- [6] Sector gates - chapter 4. [http://140.194.76.129/publications/](http://140.194.76.129/publications/eng-manuals/em1110-2-2703/toc.htm)
[eng-manuals/em1110-2-2703/toc.htm](http://140.194.76.129/publications/eng-manuals/em1110-2-2703/toc.htm), 1994.
- [7] Paulo C.F. Erbsti. *Design of Hydraulic Gates*. Springer-Verlag, 2004.
- [8] Operation manual - electromagnetic flow meter (model 801).
[http://www.valeport.co.uk/Portals/0/docs/Manuals/Current%](http://www.valeport.co.uk/Portals/0/docs/Manuals/Current%20Meters/Model%20801/0801811h.pdf)
[20Meters/Model%20801/0801811h.pdf](http://www.valeport.co.uk/Portals/0/docs/Manuals/Current%20Meters/Model%20801/0801811h.pdf), 1999.
- [9] Nortek AS. *Vectrino Velocimeter; User Guide*.
- [10] Atle Lohrmann.
- [11] G. H. Jirka and C. Lang. *Gerinnehydraulik*. Universitätsverlag Karlsruhe, 2009.
- [12] Susanne Krueger and Nils Reidar B. Olsen. Shock-wave computations in channel contractions. 2001.
- [13] H. Tennekes and J.L. Lumley. *A First Course in Turbulence*. MIT Press, 1972.
- [14] W. Rodi. *Numerische Strömungssimulation I, Grundlagen*, 2007.
- [15] Stephen B. Pope. *Turbulent flows*. Cambridge University Press, 2000.
- [16] M. Uhlmann. *Turbulenzmodelle in der Strömungsmechanik*.
<http://www.ifh.uni-karlsruhe.de/people/uhlmann>. Class notes: 2008.
- [17] J.H. Ferziger and M. Peric. *Computational Methods for Fluid Dynamics*. Springer-Verlag, 2002.
- [18] User guide - star-ccm+ version 4.02.007, 2008.
- [19] CD-adapco Peric, M. *Why STAR-CCM+ is the next step for CFD*. [http://www.](http://www.cd-adapco.com/press_room/dynamics/23/star_ccm_plus.html)
[cd-adapco.com/press_room/dynamics/23/star_ccm_plus.html](http://www.cd-adapco.com/press_room/dynamics/23/star_ccm_plus.html), 2010.
- [20] D. Apsley. *The CFD process*. [http://personalpages.manchester.ac.uk/](http://personalpages.manchester.ac.uk/staff/david.d.apsley/lectures/comphydr/cfdprocess.pdf)
[staff/david.d.apsley/lectures/comphydr/cfdprocess.pdf](http://personalpages.manchester.ac.uk/staff/david.d.apsley/lectures/comphydr/cfdprocess.pdf). 2011.

A. Data sheet

Overview of measured data			
Origo			
x 0 [m]	621173,0474		
y 0 [m]	6572629,4020		
bed [m]	z+54		
Model scale:	1:45		
River bed			
Cross-sections measured in the prototype had to be referred to the Origo			
The river geometry was divided into 4 parts and for each part a box had to be created in where the water can flow			
Step 1 Creating a body			
Setting the z-coordinates to 0, connecting the end points of each profile with a polylinie, extruding the perimeter to 3 m			
Step 2 Creating a surface area			
Using Loft command and connect each cross-section to an area			
Step 3 Creating a box			
Copying the body and the surface area in one drawing, the area is somewhere in the middle of the body, cutting bottom part so that surface area is the bed			
Boxes were added together and because of downstream part of the cross-sections had negative coordinates the whole river was shifted by Δx , Δy , Δz			
Δx [m]	1	All values had to be manipulated in respect to this transformation	
Δy [m]	3		
Δz [m]	1		
Dimensions of the dam construction			
Sector gate			
B_g [cm]	82	Width gates	
R_s [cm]	24	Radius	
B_g [cm]		H [cm]	
Flap gate middle	30,6	11,7	
Flap gate right	29,5	11,7	
Dam piers			
Numbering from east to west			
p	pier		
B_p [cm]		H_p [cm]	L_p [cm]
pier 1	5	20	34
pier 2	9,3	19	34
pier 3	4,4	18	24
pier 4	6,5	20	25
Bridge pier			
B [cm]	8		
H [cm]	23		
L [cm]	41		
R [cm]	1,5		

Flap gate

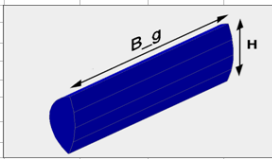
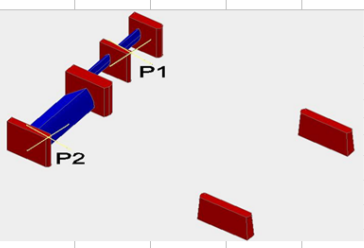


Figure A.1.: Data sheet

Right position and Height of dam construction					
For finding the right position the map: www.norgebilder.no was used					
The following two points were specified:					
Laboratory scale: (N1-y0)/45					
		Map [m]	Model [m]		
P1	N1 = x _{p1}	6572764	-1,45	Dam pier 3	
	O1 = y _{p1}	621433	5,78		
P2	N2 = x _{p2}	6572738	-2,03	Dam pier east	
	O2 = y _{p2}	621475	6,71		



The height of the dam construction was measured with a Laser in the physical model

Reference point in prototype [a.s.l]	29,48	
Reference point in model h _r [cm]	145,9	levelling instrument
h _l	laser measurements	
Δh	h _r - h _l	
h _{model}	(29,48+54)/45-Δh	

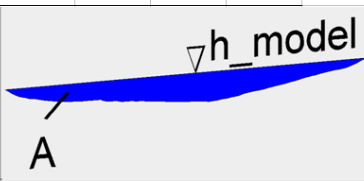
	open gates			closed gates		
	h _l [cm]	Δh [cm]	z _{model} [m]	h _l [cm]	Δh [cm]	z _{model} [m]
Sector gate	133,80	12,10	1,734	119,1	26,8	1,587
Flap gate middle	133,65	12,35	1,732	125,9	20	1,655
Flap gate west	134,10	11,80	1,737	125,75	20,15	1,654
Dam piers	141,80	4,10	1,814	141,80	4,10	1,814
Bridge pier	151,70	5,80	1,797	151,70	5,80	1,797

Water level

Reference value [a.s.l]	21
h _{model}	(21+54)/45+h _n
is the height of the water surface	
z _n is the z-coordinate of the point where the water level measurement are taken place	
h _n : water level measured with the needle	

For the closed gates:

cross-section close to	AutoCAD					
	h _n [mm]	h _{model} [m]	x _n [m]	y _n [m]	z _n [m]	
5	151,837	1,8185	7,496	18,372	1,520	
6	126,070	1,7927	5,421	13,384	1,658	
35	109,060	1,7757	8,550	5,870	1,599	
43	145,126	1,8118	10,155	2,953	1,598	
dam	113,13	1,78	6,318	-1,740	1,590	



Gate position	h _{model} [m]	z _s [m]	Q [m³/s]	A [m²]	v [m/s]
closed	1,8185	2,8185	0,092	0,534	0,172
open	1,88	2,88	0,250	0,733	0,341

Shock waves

Defining cross-section, see Fig. 4.2

Distance Origo - marked points in model [m]			Distance first point of profile 36 - marked points [m]	
Cross-section number:	Points west [m]	Points east [m]	Points west [m]	Points east [m]
9	5,315	8,63	4,175	6,279
8	5,287	8,498	4,35	6,352
7	5,247	8,428	4,522	6,444
6	5,22	8,356	4,682	6,53
5	5,195	8,286	4,869	6,638
4	5,182	8,22	5,023	6,726
3	5,14	8,16	5,168	6,825
2	5,102	8,104	5,278	6,915
1	5,02	8,035	5,478	7,014

The points were measured with a Laser distance reader

Figure A.2.: Data sheet

STAR-CCM+ / Vectrino velocimeter: velocity decomposition

The velocity measurements were conducted at profile 3, 23, 36, 51

For specifying the coordinates of the marked points in the physical model, the distance from the Origo to first point of each cross-section has to be measured

Cross-section number	L_Laser [m]	φ [°]
3	20,627	-21
23	8,818	27
36	8,462	27
51	6,779	-39

φ is the angle of each cross-section

STAR-CCM+

Defining plane sections for velocities

	Origin			Normal	
	x_o [m]	y_o [m]	z_o [m]	x_n [m]	y_n [m]
plane section	6,903760	22,824822	2,954998	-0,358368	-0,933580
plane section 2	1,437016	11,491133	3,035826	0,453990	-0,891007
plane section 3	7,665887	6,996378	2,911629	0,453990	-0,891007
plane section 4	5,934249	4,259378	2,810607	-0,629320	-0,777146

$x_n = y \sin \varphi$
 $y_n = x \cos \varphi$
 $z_n = 0$

x_o, y_o, z_o: first point of cross-section (AutoCAD)

The term plane section is used in STAR-CCM+ and stands for the corresponding cross-section

Nested Grid

For the simulations of the velocity

Block 1 include dam

Block 2 includes bridge pier

1. Creating of a new Cartesian Coordinate System

The Coordinate system was defined in the scene on the right corner of the outflow plane

	Origin [m]	i Direction [m]	j Direction [m]
x [m]	6,89628553	0,78801	0
y [m]	4,24069405	-0,615662	0
z [m]	3,51402903	0	1

2. Creating separated blocks for nested grid

	Block 1			Block 2		
	x_1 [m]	y_1 [m]	z_1 [m]	x_2 [m]	y_2 [m]	z_2 [m]
Corner 1	0	0	-0,50	1,40	0,20	-2,60
Corner 2	1,61	0,40	-0,95	1,53	0,40	-2,00

For the shock wave simulation

The block is also referred to the Cartesian Coordinate System, but displaced in x-, y- and z-direction by the factor 2, 6, 2

	Block 1			Block 2		
	x_1 [m]	y_1 [m]	z_1 [m]	x_2 [m]	y_2 [m]	z_2 [m]
Corner 1	0	0	-0,3	-1,0	0	-2,8
Corner 2	3,0	0,5	-3,0	4,0	0,5	-6,0

Water level

	Origin			Normal		φ [°]	Cross-section number in thesis
	x_o [m]	y_o [m]	z_o [m]	x_n [m]	y_n [m]		
plane section	8,1879	5,9250	2,00	-0,6293	-0,7771	-39	9
plane section 2	7,2667	6,4582	2,00	-0,6293	-0,7771	-39	8
plane section 3	7,2388	6,2794	2,00	-0,6293	-0,7771	-39	7
plane section 4	7,2185	6,1106	2,00	-0,6293	-0,7771	-39	6
plane section 5	7,1936	5,9150	2,00	-0,6157	-0,7880	-38	5
plane section 6	7,1753	5,7537	2,00	-0,6157	0,7880	-38	4
plane section 7	7,1242	5,6196	2,00	-0,6293	-0,7771	-39	3
plane section 8	7,0785	5,5195	2,00	-0,6293	-0,7771	-39	2
plane section 9	6,9766	5,3442	2,00	-0,6157	-0,7880	-38	1

Figure A.3.: Data sheet

B. Example: Simulation properties (for shock waves)

See next page.

			+-1 Custom Size	Size type	Relative to base
			`-1 Relative	Percentage of Base	20.0
Size					
				Absolute Size	0.016 m
			`-2 Trimmer	Relative/Absolute	Relative to base
Anisotropic Size					
				Custom X size	Disabled
				Custom Y size	Disabled
				Custom Z size	Disabled
			`-2 Volumetric	Part Group	[]
Control 2				Shapes	[Block 8]
			+-1 Mesh		
Conditions					
			+-1 Surface	Customize surface remesher	Enabled
Remesher					
			`-2 Trimmer	Customize isotropic size	Enabled
				Customize anisotropic size	Enabled
			`-2 Mesh Values		
			+-1 Custom Size	Size type	Relative to base
			`-1 Relative	Percentage of Base	30.0
Size					
				Absolute Size	0.024 m
			`-2 Trimmer	Relative/Absolute	Relative to base
Anisotropic Size					
				Custom X size	Disabled
				Custom Y size	Disabled
				Custom Z size	Disabled
			`-2 Physics 1	Interfaces	[]
				Regions	[Region 1]
			+-1 Models		
			+-1 Eulerian		
Multiphase					
			`-1 Eulerian		
Phases					
			+-1 H2O	Index	1
			`-1 Models		
			+-		
1 Constant Density					
			`-2 Liquid		
			`-1 H2O	Database Material	H2O (Water)
			`-		
1 Material Properties					
			+-	Method	Constant
1 Density					
			`-	Value	997.561 kg/m^3
1 Constant					
			+-	Method	Constant
2 Dynamic Viscosity					
			`-	Value	0.001002 Pa-s
1 Constant					
			+-	Method	Constant
3 Specific Heat					
			`-	Value	4181.72 J/kg-K
1 Constant					
			+-	Method	Constant
4 Speed of Sound					
			`-	Value	1500.0 m/s
1 Constant					
			`-	Method	Constant

[illegible]

			Two-Layer Delta ReY	10.0
			Convection	2nd-order
			Secondary Gradients	On
			Buoyancy Production of Dissipation	Boundary Layer Orientation
			Cmu	0.09
			C1e	1.44
			C2e	1.9
			Ct	1.0
			Sigma_k	1.0
			Sigma_e	1.2
			Sarkar	2.0
			Tke Minimum	1.0E-10
			Tdr Minimum	1.0E-10
		+-8 Reynolds-		
Averaged		Navier-Stokes		
		+-9 Segregated Flow	Convection	2nd-order
			Secondary Gradients	On
		+-10 Segregated Fluid	Continuum Temperature	300.0 K
Isothermal				
		+-11 Three		
Dimensional				
		+-12 Turbulent		
		+-13 Two-Layer All y+		
Wall Treatment				
(VOF)		`-14 Volume of Fluid	Convection	2nd-order
			Sharpening Factor	0.0
			Angle Factor	0.05
			CFL_I	0.5
			CFL_u	1.0
			Mixture density gradient	false
		+-2 Reference Values		
		+-1 Gravity	Value	[0.0, 0.0, -9.81] m/s^2
		+-2 Reference Altitude	Value	[0.0, 0.0, 0.0] m
		+-3 Minimum	Value	1.0E-6 m
Allowable Wall Distance				
		+-4 Minimum	Value	100.0 K
Allowable Temperature				
		+-5 Maximum	Value	5000.0 K
Allowable Temperature				
		`-6 Reference	Value	101325.0 Pa
Pressure				
		`-3 Initial Conditions		
		+-1 Pressure	Method	Field Function
		` -1 Field Function	Scalar Function	Pressure term
		+-2 Static	Method	Constant
Temperature				
		`-1 Constant	Value	300.0 K
		+-3 Turbulence	Method	Constant
Intensity				
		`-1 Constant	Value	0.01
		+-4 Turbulence	Method	Intensity + Viscosity Ratio
Specification				
		+-5 Turbulent Velocity	Method	Constant
Scale				
		`-1 Constant	Value	1.0 m/s
		+-6 Turbulent	Method	Constant
Viscosity Ratio				

			^-1 Constant	Value	100.0
			+7 Velocity	Coordinate System	Laboratory
				Method	Constant
			^-1 Constant	Value	[0.0, -0.341, 0.0] m/s
			-8 Volume Fraction	Method	Composite
			^-1 Composite		
			+1 ScalarProfile	Method	Field Function
			^-1 Field	Scalar Function	Initial Fluid Fraction
Function			-2 ScalarProfile	Method	Constant
			^-1 Constant	Value	0.0
			+4 Regions		
			^-1 Region 1	Index	0
				Physics Continuum	Physics 1
				Type	Fluid Region
				Mesh Continuum	Mesh 1
				Parts	[]
			+1 Boundaries		
			+1 bottom	Part Surfaces	[]
				Type	Wall
				Interfaces	
			+1 Mesh		
Conditions					
			+1 Custom	Custom curvature	Use Continuum Values
Surface Curvature					
			+2 Custom	Custom Surface Growth Rate	Disabled
Surface Growth Rate					
			+3 Custom	Custom proximity	Use Continuum Values
Surface Proximity					
			+4 Custom	Custom surface size	Disabled
Surface Size					
			-5 Customize	Disable Surface Remeshing	Disabled
Surface Remeshing					
			+2 Physics		
Conditions					
			+1 Shear Stress	Method	No-Slip
Specification					
			+2 Tangential	Method	None
Velocity Specification					
				Reference Frame	Relative To Mesh
			-3 Wall Surface	Method	Rough
Specification					
			-3 Physics Values		
			+1 Blended Wall	E	9.0
Function				Kappa	0.42
			+2 Roughness	Method	Constant
Height					
			^-1 Constant	Value	0.0020 m
			-3 Wall	B	0.0
Roughness Parameters				C	0.253
				RplusSmooth	2.25
				RplusRough	90.0
			+2 dam	Part Surfaces	[]
				Type	Wall
				Interfaces	
			+1 Mesh		
Conditions					

Surface Curvature	Custom	Custom curvature	Use Continuum Values
Surface Growth Rate	Custom	Custom Surface Growth Rate	Disabled
Surface Proximity	Custom	Custom proximity	Use Continuum Values
Surface Size	Custom	Custom surface size	Disabled
Surface Remeshing	Customize	Disable Surface Remeshing	Disabled
Conditions	Physics		
Specification	Shear Stress	Method	No-Slip
Velocity Specification	Tangential	Method	None
Specification	Wall Surface	Reference Frame	Relative To Mesh
		Method	Smooth
	Physics Values		
Function	Blended Wall	E	9.0
		Kappa	0.42
	inflow	Part Surfaces	[]
		Type	Velocity Inlet
		Interfaces	
Conditions	Mesh		
Surface Curvature	Custom	Custom curvature	Use Continuum Values
Surface Growth Rate	Custom	Custom Surface Growth Rate	Disabled
Surface Proximity	Custom	Custom proximity	Use Continuum Values
Surface Size	Custom	Custom surface size	Disabled
Surface Remeshing	Customize	Disable Surface Remeshing	Disabled
Conditions	Physics		
Direction Specification	Flow	Method	Boundary-Normal
Specification	Turbulence	Method	Intensity + Viscosity Ratio
Specification	Velocity	Method	Magnitude + Direction
	Physics Values		
Intensity	Turbulence	Method	Constant
	Constant	Value	0.01
Viscosity Ratio	Turbulent	Method	Constant
	Constant	Value	10.0
Magnitude	Velocity	Method	Field Function
Function	Field	Scalar Function	Initial Distribution
Fraction	Volume	Method	Composite
	Composite		
		Method	Field Function

```

1 ScalarProfile
|
| | | | | ^-1 Field
Function
|
| | | | | ^-
2 ScalarProfile
|
| | | | | ^-
1 Constant
|
| | | | | +-4 outflow
|
| | | | |
|
| | | | | +-1 Mesh
Conditions
|
| | | | | +-1 Custom
Surface Curvature
|
| | | | | +-2 Custom
Surface Growth Rate
|
| | | | | +-3 Custom
Surface Proximity
|
| | | | | +-4 Custom
Surface Size
|
| | | | | ^-5 Customize
Surface Remeshing
|
| | | | | +-2 Physics
Conditions
|
| | | | | +-1 Backflow
Direction Specification
|
| | | | | +-2 Target Mass
Flow Option
|
| | | | | ^-3 Turbulence
Specification
|
| | | | | ^-3 Physics Values
|
| | | | | +-1 Pressure
|
| | | | | | ^-1 Constant
|
| | | | | +-2 Turbulence
Intensity
|
| | | | | | ^-1 Constant
|
| | | | | +-3 Turbulent
Viscosity Ratio
|
| | | | | | ^-1 Constant
|
| | | | | ^-4 Volume
Fraction
|
| | | | | ^-1 Constant
|
| | | | | +-5 outflow_bottom
|
| | | | |
|
| | | | | +-1 Mesh
Conditions
|
| | | | | +-1 Custom
Surface Curvature
|
| | | | | +-2 Custom
Surface Growth Rate
|
| | | | | +-3 Custom
Surface Proximity
|
| | | | | +-4 Custom
Surface Size
|
| | | | | ^-5 Customize
Surface Remeshing
|
| | | | | +-2 Physics
Conditions
|
| | | | | +-1 Backflow
Direction Specification

```

Scalar Function	Initial Fluid Fraction
Method	Constant
Value	0.0
Part Surfaces	[]
Type	Pressure Outlet
Interfaces	
Custom curvature	Use Continuum Values
Custom Surface Growth Rate	Disabled
Custom proximity	Use Continuum Values
Custom surface size	Disabled
Disable Surface Remeshing	Disabled
Method	Boundary-Normal
Target Mass Flow Option	Disabled
Method	Intensity + Viscosity Ratio
Method	Constant
Value	0.0 Pa
Method	Constant
Value	0.01
Method	Constant
Value	10.0
Method	Constant
Value	[0.0, 0.0]
Part Surfaces	[]
Type	Pressure Outlet
Interfaces	
Custom curvature	Use Continuum Values
Custom Surface Growth Rate	Disabled
Custom proximity	Use Continuum Values
Custom surface size	Disabled
Disable Surface Remeshing	Disabled
Method	Boundary-Normal

Flow Option	+-2 Target Mass	Target Mass Flow Option	Disabled
Specification	`-3 Turbulence	Method	Intensity + Viscosity Ratio
	`-3 Physics Values		
	+-1 Pressure	Method	Constant
	`-1 Constant	Value	0.0 Pa
Intensity	+-2 Turbulence	Method	Constant
	`-1 Constant	Value	0.01
Viscosity Ratio	+-3 Turbulent	Method	Constant
	`-1 Constant	Value	10.0
Fraction	`-4 Volume	Method	Constant
	`-1 Constant	Value	[0.0, 0.0]
	+-6 outlet_small	Part Surfaces	[]
		Type	Wall
		Interfaces	
	+-1 Mesh		
Conditions			
Surface Curvature	+-1 Custom	Custom curvature	Use Continuum Values
Surface Growth Rate	+-2 Custom	Custom Surface Growth Rate	Disabled
Surface Proximity	+-3 Custom	Custom proximity	Use Continuum Values
Surface Size	+-4 Custom	Custom surface size	Disabled
Surface Remeshing	`-5 Customize	Disable Surface Remeshing	Disabled
Conditions	+-2 Physics		
Specification	+-1 Shear Stress	Method	No-Slip
Velocity Specification	+-2 Tangential	Method	None
		Reference Frame	Relative To Mesh
Specification	`-3 Wall Surface	Method	Smooth
	`-3 Physics Values		
Function	`-1 Blended Wall	E	9.0
		Kappa	0.42
	+-7 pier	Part Surfaces	[]
		Type	Wall
		Interfaces	
	+-1 Mesh		
Conditions			
Surface Curvature	+-1 Custom	Custom curvature	Use Continuum Values
Surface Growth Rate	+-2 Custom	Custom Surface Growth Rate	Disabled
Surface Proximity	+-3 Custom	Custom proximity	Use Continuum Values
Surface Size	+-4 Custom	Custom surface size	Disabled
Surface Remeshing	`-5 Customize	Disable Surface Remeshing	Disabled
Conditions	+-2 Physics		

Specification	+-1	Shear Stress	Method	No-Slip
Velocity Specification	+-2	Tangential	Method	None
Specification	-3	Wall Surface	Reference Frame	Relative To Mesh
Function	-3	Physics Values	Method	Smooth
	-1	Blended Wall		
			E	9.0
			Kappa	0.42
	+-8	top	Part Surfaces	[]
			Type	Symmetry Plane
			Interfaces	
Conditions		-1	Mesh	
Surface Curvature	+-1	Custom	Custom curvature	Use Continuum Values
Surface Growth Rate	+-2	Custom	Custom Surface Growth Rate	Disabled
Surface Proximity	+-3	Custom	Custom proximity	Use Continuum Values
Surface Size	+-4	Custom	Custom surface size	Disabled
Surface Remeshing	-5	Customize	Disable Surface Remeshing	Disabled
	-9	wall	Part Surfaces	[]
			Type	Wall
			Interfaces	
Conditions	+-1	Mesh		
Surface Curvature	+-1	Custom	Custom curvature	Use Continuum Values
Surface Growth Rate	+-2	Custom	Custom Surface Growth Rate	Disabled
Surface Proximity	+-3	Custom	Custom proximity	Use Continuum Values
Surface Size	+-4	Custom	Custom surface size	Disabled
Surface Remeshing	-5	Customize	Disable Surface Remeshing	Disabled
Conditions	+-2	Physics		
Specification	+-1	Shear Stress	Method	No-Slip
Velocity Specification	+-2	Tangential	Method	None
Specification	-3	Wall Surface	Reference Frame	Relative To Mesh
Function	-3	Physics Values	Method	Smooth
	-1	Blended Wall		
			E	9.0
			Kappa	0.42
	+-2	Feature Curves		
	+-3	Mesh Values		
	-1	Trimmer Wake		
Refinement	+-4	Physics Conditions		
Option	+-1	Initial Condition	Option	Use Continuum Values

Source Option	+-2	Momentum	Momentum Source Option	None
			Phase Source Term	Disabled
Option	+-3	Phase Source	Turbulence Source Option	None
Source Option	^-4	Turbulence	Direction	[0.0, 0.0, 1.0]
			Origin	[0.0, 0.0, 0.0] m
	^-5	Physics Values	Coordinate System	Laboratory
			Motion	Stationary
	+-1	Axis	Reference Frame	Lab Reference Frame
Specification	^-2	Motion	Mode	Single
			Scalar Field	Volume Fraction of H2O
	+-5	Derived Parts	Parts	[Region 1]
			Iso Value	0.5
	^-1	iso		
			Time-Step	0.05 s
	^-1	Value	Freeze Time	false
			Temporal Discretization	1st-order
+-6	Solvers		Solver Frozen	false
			Parallel memory optimization scaling factor	1.0
	+-1	Implicit Unsteady	Solver Frozen	false
			Reconstruction Frozen	false
	+-2	Wall Distance	Reconstruction Zeroed	false
			Temporary Storage Retained	false
	+-3	Segregated Flow	Solver Frozen	false
			Under-Relaxation Factor	0.7
	+-1	Velocity	Ramp Method	No Ramp
			Verbosity	None
Factor Ramp	+-1	Under-Relaxation	Max Cycles	30
			Parallel Migration Limit	25
Solver	^-2	AMG Linear	Extra partition-boundary sweeps	1
			Enable direct-solver	false
			Maximum direct-solver equations	32
			Convergence Tolerance	0.1
			Epsilon	0.0
			Cycle Type	Flex Cycle
			Group Size	2
			Group Size Control	Specified
			Relaxation Scheme	Gauss-Seidel
			Restriction Tolerance	0.9
			Prolongation Tolerance	0.5
			Sweeps	1
			Group Size	2
			Under-Relaxation Factor	0.3
			Pressure Reference Location	Automatic Selection
			Ramp Method	No Ramp
Factor Ramp	+-1	Under-Relaxation	Verbosity	None
			Max Cycles	30
Solver	^-2	AMG Linear		

			Parallel Migration Limit	25
			Extra partition-boundary sweeps	1
			Enable direct-solver	false
			Maximum direct-solver equations	32
			Convergence Tolerance	0.1
			Epsilon	0.0
			Cycle Type	F Cycle
			Group Size	2
			Group Size Control	Specified
			Relaxation Scheme	Gauss-Seidel
		+-1 F Cycle	Pre-Sweeps	0
			Post-Sweeps	1
			Max Levels	50
		`-2 Group Size	Group Size	2
		+-4 Segregated VOF	Under-Relaxation Factor	0.8
			Reconstruction Frozen	false
			Reconstruction Zeroed	false
			Temporary Storage Retained	false
			Solver Frozen	false
		+-1 Under-Relaxation	Ramp Method	No Ramp
Factor Ramp		`-2 AMG Linear Solver	Verbosity	None
			Max Cycles	30
			Parallel Migration Limit	25
			Extra partition-boundary sweeps	1
			Enable direct-solver	false
			Maximum direct-solver equations	32
			Convergence Tolerance	0.1
			Epsilon	0.0
			Cycle Type	F Cycle
			Group Size	2
			Group Size Control	Specified
			Relaxation Scheme	Gauss-Seidel
		+-1 F Cycle	Pre-Sweeps	0
			Post-Sweeps	1
			Max Levels	50
		`-2 Group Size	Group Size	2
		+-5 Segregated Energy	Fluid Under-Relaxation Factor	0.8
			Solid Under-Relaxation Factor	0.99
			Reconstruction Frozen	false
			Reconstruction Zeroed	false
			Temporary Storage Retained	false
			Solver Frozen	false
		+-1 Fluid Under-	Ramp Method	No Ramp
Relaxation Factor Ramp		+-2 Solid Under-	Ramp Method	No Ramp
Relaxation Factor Ramp		`-3 AMG Linear Solver	Verbosity	None
			Max Cycles	30
			Parallel Migration Limit	25
			Extra partition-boundary sweeps	1
			Enable direct-solver	false
			Maximum direct-solver equations	32
			Convergence Tolerance	0.1
			Epsilon	0.0
			Cycle Type	F Cycle

			Group Size	2
			Group Size Control	Specified
			Relaxation Scheme	Gauss-Seidel
		+-1 F Cycle	Pre-Sweeps	0
			Post-Sweeps	1
			Max Levels	50
		`-2 Group Size	Group Size	2
	+-6	K-Epsilon Turbulence	Under-Relaxation Factor	0.8
			Reconstruction Frozen	false
			Reconstruction Zeroed	false
			Temporary Storage Retained	false
			Solver Frozen	false
		+-1 Under-Relaxation	Ramp Method	No Ramp
Factor Ramp		`-2 AMG Linear Solver	Verbosity	None
			Max Cycles	30
			Parallel Migration Limit	25
			Extra partition-boundary sweeps	1
			Enable direct-solver	false
			Maximum direct-solver equations	32
			Convergence Tolerance	0.1
			Epsilon	0.0
			Cycle Type	Flex Cycle
			Group Size	2
			Group Size Control	Specified
			Relaxation Scheme	Gauss-Seidel
		+-1 Flex Cycle	Restriction Tolerance	0.9
			Prolongation Tolerance	0.5
			Sweeps	1
		`-2 Group Size	Group Size	2
	`-7	K-Epsilon Turbulent	Under-Relaxation Factor	1.0
Viscosity			Maximum Ratio	100000.0
			Solver Frozen	false
	+-7 Stopping Criteria			
	+-1 Maximum Inner		Max Inner Iterations	5
Iterations			Enabled	true
			Criterion Satisfied	false
			Logical Rule	Or
	+-2 Maximum Physical		Max Physical Time	150.0 s
Time			Enabled	true
			Criterion Satisfied	false
			Logical Rule	Or
	+-3 Maximum Steps		Maximum Steps	1000
			Enabled	false
			Criterion Satisfied	false
			Logical Rule	Or
	`-4 Stop File		Stop Inner Iterations	true
			Path	ABORT
			Enabled	true
			Criterion Satisfied	false
			Logical Rule	Or
	+-8 Reports			
	`-1 iso_surface_z		Scalar Field Function	Position[Z]

		Parts	[iso]
		Units	m
+-9	Monitors	Monitors To Print	[Continuity, X-momentum, Y-momentum, Z-momentum, H2O, Energy, Tke, Tdr]
		Output Direction	Horizontal
		Heading Print Frequency	10
+-10	Representations		
	+-1 Import	Faces	69134
		Edges	0
	`-1 Regions		
	`-1 Region 1	Faces	69134
		Edges	0
	+-1 Boundaries		
	+-1 bottom	Faces	67885
	+-2 dam	Faces	252
	+-3 inflow	Faces	228
	+-4 outflow	Faces	2
	+-	Faces	18
5	outflow_bottom		
	+-6 outlet_small	Faces	2
	+-7 pier	Faces	61
	+-8 top	Faces	109
	`-9 wall	Faces	577
	`-2 Feature Curves		
	+-2 Remeshed Surface	Faces	493242
		Edges	0
	`-1 Regions		
	`-1 Region 1	Faces	493242
		Edges	0
	+-1 Boundaries		
	+-1 bottom	Faces	351162
	+-2 dam	Faces	9443
	+-3 inflow	Faces	2707
	+-4 outflow	Faces	1024
	+-	Faces	5366
5	outflow_bottom		
	+-6 outlet_small	Faces	1181
	+-7 pier	Faces	2067
	+-8 top	Faces	66074
	`-9 wall	Faces	54218
	`-2 Feature Curves		
	`-3 Volume Mesh	Cells	3204247
		Interior Faces	9595504
		Vertices	3457987
	+-1 Finite Volume		
Regions	`-1 Region 1	Cells	3204247
		Interior Faces	9595504
		Vertices	3457987
	`-1 Finite Volume		
Boundaries	+-1 bottom	Faces	199938
	+-2 dam	Faces	10443
	+-3 inflow	Faces	1072
	+-4 outflow	Faces	403
	+-		

5	outflow_bottom	Faces	5347
	+-6 outlet_small	Faces	933
	+-7 pier	Faces	2165
	+-8 top	Faces	26743
	-9 wall	Faces	36447
	-2 Cell Sets		
+-11	Coordinate Systems		
+-12	Tables		
	-1 XyzInternalTable 1	Coordinate System	Laboratory
		Parts	[iso]
		Scalars	[Position[Z]]
		Extracted	[Position[Z], X, Y, Z]
+-13	Units	Preferred System	Système Internationale
+-14	Field Functions		
	+-1 Initial Distribution	Type	Scalar
		Function Name	Initial Distribution
		Definition	(\$Position[2]<=3.88)?0.341:0
		Ignore Boundary Values	false
		Assembly code	(if (<= \$Position[2] 3.88) 0.341 0)
	+-2 Initial Fluid Fraction	Type	Scalar
		Function Name	Initial Fluid Fraction
		Definition	(\$Position[2]<=3.88)?1:0
		Ignore Boundary Values	false
		Assembly code	(if (<= \$Position[2] 3.88) 1 0)
	+-3 Pressure term	Type	Scalar
		Function Name	Pressure term
		Definition	(\$Position[2]<=3.88)? (1000*9.81*3.88- 1000*9.81*\$Position[2]):0
		Ignore Boundary Values	false
		Assembly code	(if (<= \$Position[2] 3.88) (- 38062.8 (* 9810 \$Position[2])) 0)
+-15	Volume Shapes		
	+-1 Block 1	Coordinate System	Laboratory->Cartesian 1
		Corner1	[0.0, 0.0, -0.3] m,m,m
		Corner2	[3.0, 0.5, -3.0] m,m,m
	+-2 Block 2	Coordinate System	Laboratory->Cartesian 1
		Corner1	[0.01, 0.0, -1.2] m,m,m
		Corner2	[2.0, 0.4, -0.95] m,m,m
	+-3 Block 3	Coordinate System	Laboratory->Cartesian 1
		Corner1	[0.15, 0.0, -1.3] m,m,m
		Corner2	[2.1, 0.4, -1.2] m,m,m
	+-4 Block 4	Coordinate System	Laboratory->Cartesian 1
		Corner1	[0.17, 0.0, -1.7] m,m,m
		Corner2	[2.18, 0.4, -1.3] m,m,m
	+-5 Block 5	Coordinate System	Laboratory->Cartesian 1
		Corner1	[0.45, 0.0, -2.0] m,m,m
		Corner2	[2.3, 0.4, -1.7] m,m,m
	+-6 Block 6	Coordinate System	Laboratory->Cartesian 1
		Corner1	[0.59, 0.0, -2.5] m,m,m
		Corner2	[2.3, 0.4, -2.0] m,m,m
	+-7 Block 7	Coordinate System	Laboratory->Cartesian 1
		Corner1	[1.6092, 0.0, -0.95] m,m,m
		Corner2	[1.8, 0.4, -0.6] m,m,m
	-8 Block 8	Coordinate System	Laboratory->Cartesian 1

	Corner1	[-1.0, 0.0, -2.8] m,m,m
	Corner2	[4.0, 0.5, -6.0] m,m,m
+--16 User Code		
+--17 Data Set Functions		
+--18 GT-POWER	GT-POWER Directory Name	
	GT-POWER Case Name	
+-1 GT-POWER Species		
`--2 GT-POWER Zones		
+--19 Data Mappers		
+--20 Reference Frames		
`--1 Lab Reference Frame		
+--21 Motions		
`--1 Stationary		

Solution

Accumulated CPU Time over all processes (s) 810735.3260000153
Elapsed Time (s) 135096.00744456588
Time Level 2877
Solution Time 143.89999999999847

